Graphical Abstract (for review)

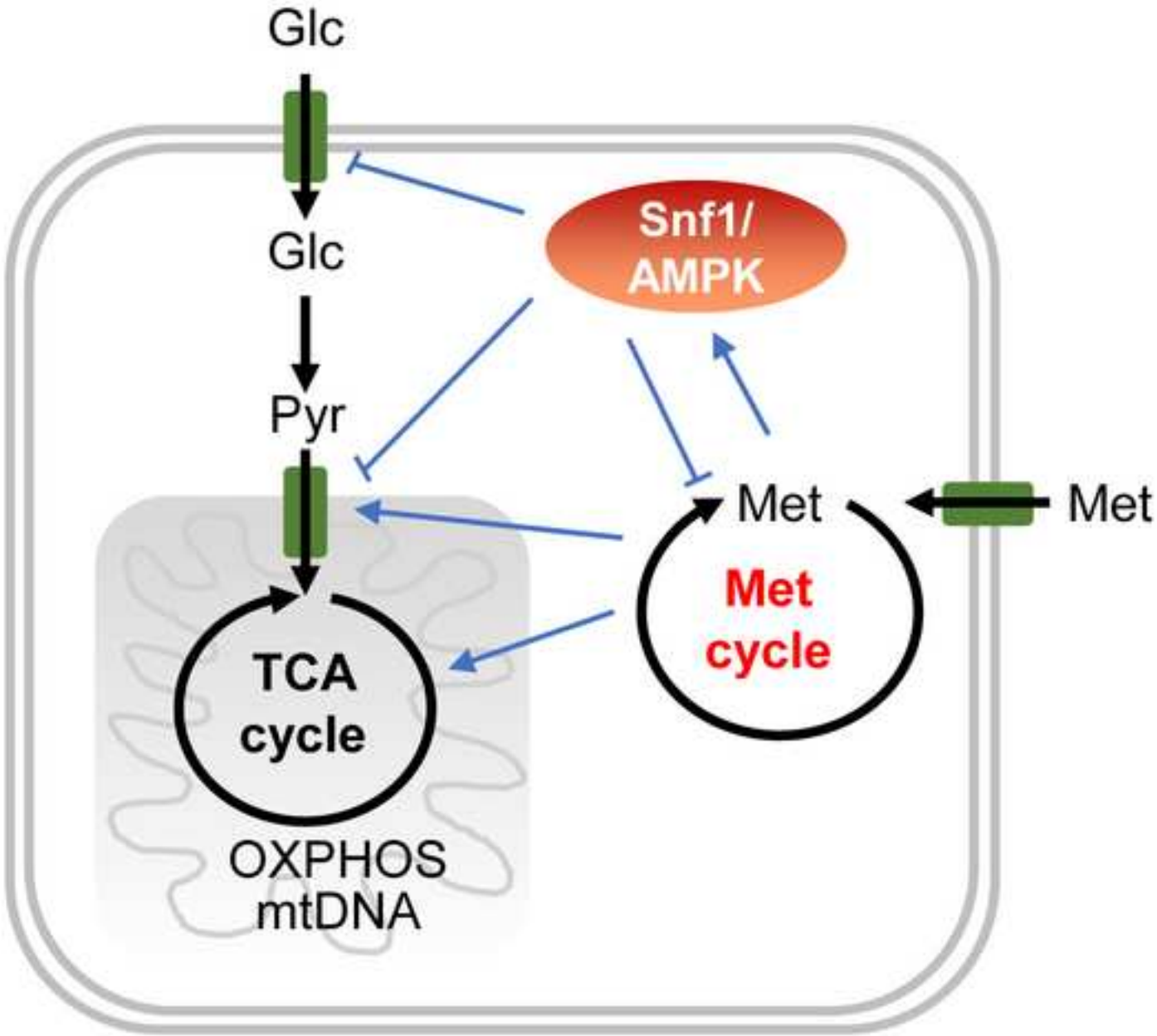

Highlights

- Methionine supplementation increases mitochondrial functions
- Methionine addition enhances mitochondrial pyruvate uptake and TCA cycle activity
- Loss of pyruvate transport in *snf1*Δ cells is detrimental in methionine condition

Methionine Supplementation Stimulates Mitochondrial Respiration

Farida Tripodi[1,2*], Andrea Castoldi[1,∫*], Raffaele Nicastro[1,#], Veronica Reghellin[1,∫], Linda Lombardi[1] Cristina Airoldi[1,2], Ermelinda Falletta[3], Elisa Maffioli[4], Pasquale Scarcia[5], Luigi Palmieri[5], Lilia Alberghina[1,2], Gennaro Agrimi[5**], Gabriella Tedeschi[4**], Paola Coccetti[1,2**]

[1]Department of Biotechnology and Biosciences, University of Milano-Bicocca, Milan, Italy

[2]SYSBIO, Centre of Systems Biology, Milan, Italy

[3]Department of Chemistry, University of Milano, Milan, Italy

[4]DIMEVET – Department of Veterinary Medicine- University of Milano, Milan, Italy

[5] Department of Biosciences, Biotechnology and Biopharmaceutics, University of Bari, Italy

[#] Present address: Department of Biology, University of Fribourg, Fribourg, Switzerland

[∫] Present address: Eurofins BioPharma, Vimodrone, Italy

* These authors contributed equally to this work

** To whom correspondence should be addressed:

paola.coccetti@unimib.it; gabriella.tedeschi@unimi.it; gennaro.agrimi@uniba.it

Keywords: Snf1/AMPK, metabolomics, shotgun proteomics, MPC (Mitochondrial Pyruvate Carrier), *Saccharomyces cerevisiae*, S-adenosyl-methionine.

Abstract

Mitochondria play essential metabolic functions in eukaryotes. Although their major role is the generation of energy in the form of ATP, they are also involved in maintenance of cellular redox state, conversion and biosynthesis of metabolites and signal transduction. Most mitochondrial functions are conserved in eukaryotic systems and mitochondrial dysfunctions trigger several human diseases.

By using multi-omics approach, we investigate the effect of methionine supplementation on yeast cellular metabolism, considering its role in the regulation of key cellular processes. Methionine supplementation induces an up-regulation of proteins related to mitochondrial functions such as TCA cycle, electron transport chain and respiration, combined with an enhancement of mitochondrial pyruvate uptake and TCA cycle activity. This metabolic signature is more noticeable in cells lacking Snf1/AMPK, the conserved signalling regulator of energy homeostasis. Remarkably, *snf1Δ* cells strongly depend on mitochondrial respiration and suppression of pyruvate transport is detrimental for these cells in methionine condition, indicating that respiration mostly relies on pyruvate flux into mitochondrial pathways.

These data provide new insights into the regulation of mitochondrial metabolism and extends our understanding on the role of methionine in regulating energy signalling pathways.

Introduction

To tackle the central cell biology issue of how a specific genotype is able to generate a given phenotype in certain environmental conditions, a useful approach is to start by unravelling the complexity of the phenotypic features generated by the interacting genetic and nutritional perturbations. Here, we approach this issue by considering Snf1/AMPK, the key signalling regulator of energy homeostasis in eukaryotes [1] and the amino acid methionine, an essential player of the one-carbon metabolism [2]. In *Saccharomyces cerevisiae* Snf1 protein complex is a central component of glucose signalling pathway. It promotes respiratory metabolism and gluconeogenesis, being necessary for growth in low glucose or alternative carbon sources [3]. It is made by the catalytic α subunit (Snf1), the γ subunit (Snf4) and one of the three alternative β subunits (Sip1, Sip2, Gal83), which determine the intracellular localization of the kinase [3,4]. Snf1/AMPK is active when the catalytic α subunit is phosphorylated on Thr210 by one of the three constitutive active kinases Sak1, Tos3 or Elm1 [5]. Snf1 activation requires also the association between α and γ subunits, which stabilizes the active conformation of the kinase [5]. In response to high glucose concentrations, Snf1 is inactivated through de-phosphorylation of Thr210 by the phosphatase Glc7/Reg1 [6,7]. Phosphorylation of Ser214, inside the activation loop, has been reported as an additional mechanism for downregulating Snf1/AMPK kinase activity [8].

Upon activation, Snf1 phosphorylates a number of transcription factors, activating some and repressing others [3]. Specifically, active Snf1 causes the translocation to the cytoplasm of Mig1, thus leading to the expression of glucose repressed-genes [9,10]. Besides Mig1, Snf1 activates Cat8 and Sip4, which regulate the expression of gluconeogenic genes [11,12], and Adr1, which activates the expression of the alcohol dehydrogenase gene *ADH2* and genes of glycerol metabolism, fatty acid utilization and peroxisome biogenesis [13,14]. Snf1 also phosphorylates and regulates the nuclear localization of Hcm1, a forkhead transcription factor, leading to increased

transcription of genes involved in respiration during nutrient scarcity [15]. Furthermore, Snf1 stimulates the activity of several metabolic enzymes, such as the glycerol-3-phosphate dehydrogenase isoform Gpd2 [16] and the acetyl-CoA carboxylase Acc1 [17,18]. Although Snf1/AMPK function has been mostly studied in respiration-dependent growth [19–21], some reports indicate that it is active even in glucose repression [22–24]. In keeping with these data, we recently reported that Snf1/AMPK phosphorylation on Thr210 is slightly detectable also in high glucose [25] and, in this condition, it regulates G1/S cell-cycle transition, proper spindle orientation and cellular metabolism [25–28]. Moreover, Snf1/AMPK interacts with and phosphorylates the adenylate cyclase Cyr1 in a nutrient-independent manner and negatively regulates intracellular cAMP content as well as PKA-dependent transcription [29].

The sulfur amino acid methionine (Met) is the precursor of S-adenosylmethionine (SAM), the universal cellular methyl donor [30–33]. Methionine metabolism regulates key biological functions in mammalian cells, such as cell proliferation, metabolism, stem cell maintenance and embryonic development [34,35]. It is well-known that methionine-restriction extends lifespan across different species [36] and in human fibroblast this is due to a decrease of mitochondrial oxidative phosphorylation [37]. Importantly, SAM is involved in G1 cell-cycle regulation in yeast [38] and stimulation of SAM synthesis triggers Snf1 activation in yeast [39].

Here, we have uncovered new links between methionine metabolism and the Snf1/AMPK pathway. By using metabolomics profiling, metabolic flux analysis and mitochondrial proteomics, we have discovered a novel function for Snf1/AMPK as a negative regulator of aerobic respiration and mitochondrial pyruvate uptake, in methionine and glucose-repressing conditions.

Results

Methionine addition affects proliferation and metabolism in the absence of Snf1

Stimulation of S-adenosylmethionine (SAM) synthesis leads to Snf1 activation [39]. Accordingly, Snf1-dependent phosphorylation of an acetyl-coenzyme A carboxylase 1 derived reporter [40] increased upon methionine supplementation (Fig. 1A).

Then, to better understand the relation between methionine metabolism and Snf1 activity, the prototrophic *CEN.PK JT4 snf1Δ* strain and its control wild type were grown on synthetic medium containing 2% glucose and increasing concentrations of methionine (from 0.05 g/l up to 1.5 g/l). Methionine and SAM supplementation (Fig. 1B, Supplementary Fig. S1A) affected both proliferation and budding index of cells lacking Snf1 (Fig. S1B).

Addition of methionine (0.1 g/l, 0.67 mM), which was uptaken at similar rates by wt and *snf1Δ* strains, significantly impaired glycerol secretion in cells lacking Snf1, while no alterations were observed on glucose uptake, ethanol, acetate and glycerol secretion rates, which were already lower in the *snf1Δ* mutant (Fig. 1C).

To gain more insight into the relevant intracellular metabolic changes upon *SNF1* deletion and methionine addition, we next performed a metabolomic profiling analysis (Fig. 2A, Supplementary Fig. S2A-B, Supplementary Table S1). In the control strain grown in the presence of methionine, most metabolites decreased, mainly amino acids, intermediates of the citric acid cycle and the urea cycle (Fig. 2A, Supplementary Fig. S2B). On the contrary, *SNF1* deletion, in combination with methionine addition, promoted an increase in the level of amino acids, tricarboxylic acids, as well as TCA cycle derivatives and urea cycle intermediates, with only few exceptions (Fig. 2A, Supplementary Fig. S2B). One of the most upregulated metabolites was trehalose, which was more abundant in *snf1Δ* cells compared to wt, and was strongly up-regulated in the presence of

methionine (Fig. 2A, Supplementary Fig. S2B), possibly due to the increased activity of trehalose-6-phosphate synthase upon methylation [41].

Interestingly, intracellular homocysteine increased in cells lacking Snf1 (Fig. 2A, Supplementary Fig. S2B) and all metabolites of the methionine cycle were more up-regulated in the *snf1Δ* mutant supplemented with methionine in comparison with the control (Fig. 2A-C). Moreover, in this condition, S-adenosylmethionine and S-adenosylhomocysteine ratio (SAM/SAH) decreased in the wild type, while increased in the *snf1Δ* mutant, further confirming the unbalance of methionine metabolism due to Snf1 loss (Fig. 2D).

Taken together, these data indicate that methionine supplementation induces a general remodelling of metabolism, being more evident in cells lacking Snf1.

Mitochondrial proteome shows an increase of proteins involved in aerobic respiration in methionine medium

To gain a better insight in the up-regulation of TCA cycle intermediates following *SNF1* deletion and methionine treatment, a label-free shotgun proteomics approach was used to investigate the mitochondrial proteome of wild type and *snf1Δ* cells grown without and with methionine. The corresponding Venn diagram and workflow are shown in Fig. 3A and Supplementary Fig. S3, respectively. Among the 1236 proteins common to all data sets, Supplementary Table S2 reports only the proteins whose differences were statistically significant according to ANOVA test. More than 89% of them were reported as mitochondrial according to Yeast Mine software and [42], indicating a significant enrichment in mitochondrial components. Remarkably, Snf1 was found associated to mitochondria, further confirming its mitochondrial localization [43]. Due to the high sensitivity of the analysis, non-mitochondrial proteins were also identified, as previously reported [42], mainly localized in compartments tightly associated to mitochondria (such as endoplasmic reticulum, Golgi and vacuole). A principal component analysis (PCA), carried out on the four data

sets (wt, wt + M, *snf1Δ*, *snf1Δ* + M) confirmed that, as expected, each condition exerted a specific detectable effect on protein expression. However, the proteome of both wt and *snf1Δ* moved towards negative values of the Component 1 upon methionine addition (Fig. 3B).

We then carried out pairwise analyses focusing on the following comparisons: *snf1Δ*/wt (Fig. 3C, Supplementary Table S3), wt + M/wt (Fig. 3D, Supplementary Table S4), *snf1Δ* + M/*snf1Δ* (Fig. 3E, Supplementary Table S5) and *snf1Δ* + M/wt + M (Fig. 3F, Supplementary Table S6). *SNF1* deletion mostly induced an up-regulation of many proteins related to cellular transport (transmembrane transport, mitochondrial transport, late endosome to vacuole transport, Golgi to endosome transport, heme transport) and amino acids biosynthesis (cellular amino acid biosynthetic process, glutamate biosynthetic process, serine family amino acid biosynthetic process) (Fig. 3C, Supplementary Table S3), in keeping with metabolomics analysis (Fig. 2) and with previously reported transcriptional up-regulation of genes related to transport, amino acids biosynthesis and iron homeostasis of the *snf1Δ* mutant [26].

Methionine induced a down-regulation of proteins involved in sterol and ergosterol biosynthesis only in *snf1Δ* mutant (Fig. 3E, Supplementary Table S5). In addition, proteins involved in ribosome biogenesis and RNA processing were down-regulated in both wt and *snf1Δ* cells (Fig. 3D, E and Supplementary Tables S4-S5). The identification of this class of proteins is not surprising, in keeping with previous data showing the association of ribosomes with mitochondria [42,44].

Remarkably, in both strains methionine induced an up-regulation of proteins related to mitochondrial functions, such as TCA cycle (*i.e.* Mdh1, Sdh1,2,4, Cit1, Idh2, Idp1), electron transport chain and aerobic respiration (*i.e.* Cyt1, Qcr2,7,10, Cir2, Cyb2, Cor1, Cyc1, Rip1, Mam33), as well as proteins related to redox processes (Fig. 3D-E and Supplementary Tables S4-S5), being more up-regulated in *snf1Δ* mutant (Fig. 3F, Supplementary Table S6).

Therefore, proteins related to mitochondrial respiration increase in methionine-medium.

Methionine addition stimulates mitochondrial respiration in the absence of Snf1

To test whether methionine supplementation and *SNF1* deletion were involved in the regulation of mitochondrial activity, we measured several parameters associated to active mitochondria. Loss of *SNF1* determined a striking increase of mtDNA copy number, mitochondrial membrane potential, as well as oxygen consumption of mitochondria isolated from cells grown in methionine-supplemented media (Fig. 4A-C). In details, although mitochondria isolated from *snf1Δ* mutant oxidized succinate and NADH to rates comparable to those of the control, they displayed a higher oxidation rate when NADH was used as a substrate in cells grown in methionine medium (Fig. 4C). In keeping with the higher respiration rate, antimycin A, an inhibitor of the mitochondrial electron transport chain complex III [45,46], had a dramatic impact on the growth rate of the *snf1Δ* mutant in the presence of methionine (Fig. 4D).

Despite the more sustained mitochondrial metabolism, intracellular basal ATP levels decreased upon *SNF1* deletion in combination with methionine (Fig. 4E), indicating that energy consuming processes, *i.e.* fatty acids and lipid droplets accumulation (Fig. 2A and Supplementary Fig. S4A, respectively), trehalose (Fig. 2A) and SAM biosynthesis (Fig. 2D) were draining energy in this growth condition.

Altogether, these data confirm that methionine has a relevant effect on the metabolism of cells lacking Snf1, highlighting its essential involvement in mitochondrial respiration.

Methionine addition stimulates pyruvate transport into mitochondria in the absence of Snf1

To gain further insight into mitochondrial substrate utilization, we cultured cells in the presence of [U-$^{13}C_6$] glucose and determined steady-state isotopic labelling from which important intracellular flux partitioning ratios were calculated [47]. Then, a metabolic flux analysis was performed integrating these intracellular flux ratios (Supplementary Fig. S5A), consumption and secretion rates (Fig. 1C) in a yeast model of central carbon metabolism [47,48] (Fig. 5A, Supplementary Fig.

187 S5B). *snf1Δ* mutant displayed a larger flux of carbon towards mitochondria as compared to the
188 control, showing more pyruvate transported into these organelles in both conditions (Fig. 5B,
189 Supplementary Fig. S5B). Strikingly, in methionine supplementation, pyruvate transport towards
190 mitochondria, TCA cycle activity and respiration were more up-regulated in the *snf1Δ* mutant than
191 wt (Fig. 5A-C, Supplementary Fig. S5B).
192 The fraction of oxaloacetate (OAA) generated from mitochondrial malate by malate
193 dehydrogenase (*i.e.* oxidative TCA cycle activity) [49] was then calculated. As expected, in the wild
194 type, under glucose repression, TCA cycle oxidative activity was low [49] and increased from 4.6%
195 to 21.5% in methionine growth condition (Fig. 5C). In contrast, a lower glucose-repressed
196 metabolism was detectable in the *snf1Δ* mutant, being oxidative TCA cycle activity 29.25% without
197 methionine and raising up to 47% in the presence of methionine (Fig. 5C).
198 The downregulation of glycerol secretion suggested a sustained mitochondrial oxidation of
199 cytosolic NADH in the presence of methionine in cells lacking Snf1 (Fig. 1C). Remarkably, the
200 model predicted an increase of the oxygen consumption in the *snf1Δ* cells (Fig. 5A, Supplementary
201 Fig. S5B), in accordance with the stimulation of mitochondrial respiration in cells lacking Snf1
202 above reported (Fig. 4C).
203 Overall, our results support an inhibitory function of Snf1/AMPK on respiration as well as on TCA
204 cycle in glucose repressed conditions, further enforced in methionine-medium.
205 *Mpc1 function has a key role for methionine-dependent respiratory activity in the absence of Snf1*
206 Overall our data indicate that methionine stimulates mitochondrial pyruvate transport and
207 respiration. Therefore, we examined the level of the three subunits of the MPC (Mitochondrial
208 Pyruvate Carrier) complex in strains expressing HA-tagged versions of Mpc1,2,3. While Mpc1
209 levels were almost unchanged, the level of Mpc2 and Mpc3 strongly increased in methionine
210 supplementation, both in wt and *snf1Δ* cells (Fig. 6A), suggesting that the increased mitochondrial

functionality may depend on the upregulation of MPC subunits. However, although the effect of methionine was similar in both strains, mitochondrial respiration was physiologically more noticeable in cells lacking Snf1 (Fig. 4). Thus, we treated cells with UK5099, which covalently binds to MPC and blocks pyruvate transport [50]. While only a slight decrease of proliferation was observed in both strains, a dramatic slow-down of growth rate occurred in cells lacking Snf1 in the presence of methionine (Fig. 6B).

Loss of the major structural subunit of the mitochondrial pyruvate carrier, Mpc1, results in defective mitochondrial pyruvate uptake [51,52]. Thus, we tested the effect of *MPC1* deletion on the *snf1Δ* mutant grown with and without methionine in the medium. *mpc1Δ* cells grew slower than the control, as previously reported [51], also in the presence of methionine (Fig. 6C). Remarkably the s*nf1Δmpc1Δ* double mutant had a major growth defect only in methionine medium (Fig. 6C), in accordance with data obtained with the inhibitor UK5099 (Fig. 6B). The strong reliance on pyruvate transport and respiration of *snf1Δ* cells was further confirmed by the complete growth arrest of the s*nf1Δmpc1Δ* mutant treated with Antimycin A (Fig. 6D), which however had no effect on cellular viability (data not shown).

Taken together, our results indicate that respiration due to Snf1 loss mostly relies on the flux of pyruvate into mitochondria.

Discussion

Methionine cycle, being a key metabolic network which integrates biosynthesis, one-carbon metabolism and epigenetics, regulates important biological functions such as cell proliferation, metabolism, stem cell maintenance and embryonic development [34,35]. For these reasons and also because its regulation is mostly unknown, methionine metabolism still needs to be investigated deeper. In the present study, we showed that methionine metabolism has a strong impact on cellular and metabolic features of proliferating yeast cells, collecting evidences that most of them are tightly connected with Snf1/AMPK.

Snf1/AMPK, an important cellular energy sensor, is conserved from yeast to humans [1]. In yeast, it is required for the expression of glucose-repressed genes and cells lacking Snf1 are unable to grow on non-fermentable carbon sources, such as glycerol or ethanol. Paradoxically, while in the absence of glucose Snf1 is required to increase respiration, in high glucose condition, oxidative phosphorylation sustains growth and energy production in *snf1Δ* cells [26], indicating an unconventional role of Snf1 under glucose repression. Here we showed that although methionine supplemented to the medium was rather low (0.1 g/L) and ineffective to inhibit wild type growth ([53], Fig. 1B), in cells lacking Snf1, it induced a general slow-down of proliferation, combined with enhanced mitochondrial DNA, NADH oxidation, TCA cycle flux, and mitochondrial pyruvate uptake (summarized in Fig. 7).

Notably, an imbalance of methionine cycle was evident in cells lacking Snf1 even in methionine-free medium. In fact, intracellular homocysteine, a thiol amino acid, whose dysfunction is associated with a multitude of human diseases [54], increased in *snf1Δ* cells and all metabolites of this cycle as well as methylation potential (SAM/SAH) were further up-regulated in the presence of methionine (Fig. 2). In support of this, methionine metabolism has been recently reported to be tightly connected with Snf1/AMPK since SAM accumulation enhances Snf1 activation [39],

highlighting also a Snf1-dependent function in fine tuning methionine metabolism in a feedback loop (Fig. 7).

More interestingly, although in methionine medium many proteins involved in electron transport chain and aerobic respiration were up-regulated both in wild type and in *snf1Δ* cells (Fig. 3D-E), inhibition of mitochondrial respiration was detrimental only for cells lacking Snf1 (Fig. 4D), indicating a reliance on mitochondrial function, further supported by the up-regulation of redox processes only in that condition (Fig. 3F).

Thus, our results clearly indicate that the addition of a small amount of methionine in the medium has a strong impact only if Snf1/AMPK is inactive and provides novel insights into methionine-dependent regulation of proliferation and mitochondrial metabolism.

Several lines of evidences support the connection between methionine metabolism and mitochondrial function: *i)* metabolism of yeast strains with high intracellular SAM content [55] depends on elevated TCA cycle fluxes and respiration activity [56]; *ii)* homocysteine metabolism regulates mitochondrial respiration in T cells and mitochondrial membrane potential in yeast [57,58]; *iii)* in human fibroblast, the activity of oxidative phosphorylation by complex IV decreases in methionine restriction, due to the reduced *COX1* level [37].

In support of these data, we confirm the connection between methionine metabolism and mitochondrial respiration showing, in addition, the key role of Snf1/AMPK in such a regulation.

It is well known that in glucose containing medium, yeast cells metabolize glucose predominantly through glycolysis, followed by alcoholic fermentation. Since glucose represses functions connected to TCA cycle and respiration, only a relatively small fraction of glycolytically produced pyruvate is translocated into mitochondria and converted to acetyl-CoA. Our metabolic flux analysis indicates that methionine supplementation stimulates pyruvate transport into mitochondria in glucose-repressing conditions (Fig. 5). Remarkably, s*nf1Δmpc1Δ* mutant shows a

277 slow growth phenotype in methionine medium (Fig. 6C), highlighting the physiological relevance
278 of Mpc1 function in cells lacking Snf1.
279 The activity of the Mpc1 carrier is crucial to determine the fate of pyruvate, it is involved in the
280 triggering of the Warburg effect and is considered a potential target for cancer therapy [59].
281 Moreover, the role of protein kinase AMPK in the regulation of *MPC1* expression has recently
282 emerged [60]. Decreased *MPC1* expression promotes the maintenance of stemness of cancer cells,
283 which become more migratory and resistant to both chemotherapy and radiotherapy [61,62].
284 Conversely, the inhibition of pyruvate mitochondrial transport by MPC inhibitor UK5099 activates
285 AMPK [63]. Collectively, the above studies, together with our data, support a new link between
286 AMPK pathway and mitochondrial pyruvate transport. Strikingly, the coexistence of glycolysis and
287 functional TCA cycle activity and OXPHOS offers a selective metabolic advantage for cancer cell
288 proliferation and tumorigenesis [64,65]. Moreover, some studies highlight the double-edged
289 function of AMPK in the regulation of tumorigenic potential, showing either an anti-tumorigenic or
290 a pro-tumorigenic function [66,67]. Therefore, in future studies it will be interesting to dissect the
291 molecular mechanism of pyruvate metabolism by Snf1/AMPK along with its conservation in
292 eukaryotic systems.
293 Besides respiratory function, in *snf1Δ* cells grown in the presence of methionine, there was also a
294 significant decrease of several proteins involved in ergosterol biosynthesis, among which Erg1,
295 Erg4, Erg6 and Scs7. Remarkably, mutants with deficiency in ergosterol biosynthesis accumulate S-
296 adenosylmethionine [55], in accordance with our data showing a significant increase of this
297 metabolite in *snf1Δ* cells (Fig. 2C). Moreover, the down-regulation of *SAH1* expression impairs
298 sterol synthesis, leading to a 4-fold elevated squalene levels [54]. Egr1, involved in squalene
299 biosynthesis, is downregulated in cells lacking Snf1, which also show S-adenosylhomocysteine
300 accumulation (Fig. 2C).

Interestingly, the proteomics analysis also highlights the down-regulation of glycosylation and vacuolar transport processes in *snf1Δ* cells grown in methionine condition (Fig. 5F, Supplementary Table S6). Kar2, the ATPase involved in protein import/export into the ER [68], was down-regulated too, in accordance with studies reporting the involvement of Snf1 in ER stress response [69–71].

Finally, histone deacetylation proteins were down-regulated in the absence of Snf1 (Fig. 3C, Supplementary Table S3). It was previously reported that inactivation of *SNF1* globally decreases intracellular pool of acetyl-CoA as well as histone acetylation [72]. Therefore, we hypothesize that the downregulation of histone deacetylation functions here presented could be a consequence of the reduced level of acetylation in the *snf1Δ* strain [72].

Taken together, our results shed significant light on the interplay among Snf1/AMPK activity, methionine and mitochondrial metabolism in glucose-repressing conditions and extend our mechanistic understanding of how methionine can influence cell fate.

Material and methods

Yeast strains and growth conditions

S. cerevisiae strains used in this study are reported in Table 1. Synthetic medium (SD) contained 2% glucose, 6.7 g/L of Yeast Nitrogen Base without amino acids (Difco). Methionine was added to the concentrations indicated in figure legends. In these conditions, cells exhibit exponential growth between OD_{600nm} = 0.1 (approximately equivalent to $2*10^6$ cells/ml) and OD_{600nm} = 2.5 ($5*10^7$ cells/ml); all experiments were performed in exponential phase of growth (OD_{600nm}0.5-1). Antimycin A was added to a final concentration of 1 µg/ml from 2 mg/ml stock in 100% ethanol, UK5099 was added to a final concentration of 50 µM from 10 mM stock in 100% DMSO; the same volume of solvent was added in the control cultures. To evaluate Snf1 activity, phosphorylation of the reporter ACC1-HA was assayed in a strain transformed with the plasmid pYX242-ACC1-GFP-HA (or pYX242-ACC1-S79A-GFP-HA as negative control) [40].

Protein extraction and immunoblotting

Cells were harvested by filtration and lysed in 250 µl ice-cold lysis buffer (50 mM Tris pH 7.5, 150 mM NaCl, 0.1, Nonidet p-40, 10% glycerol) with 1 mM PMSF, protease inhibitor mix (Complete EDTA free protease inhibitor mixture tablets; Roche) and phosphatase inhibitor mix (Cocktail II, Sigma-Aldrich). An equal volume of acid-washed glass beads (Sigma-Aldrich) was added before disruption. Cells were broken by 20 cycles of vortex and ice of 1 min each. Protein concentration was determined with Bio-Rad protein assay. After addition of SDS-sample buffer, crude extract was boiled at 98 °C for 5 min.

Anti-phospho-Acetyl-CoA Carboxylase (Ser79) antibody (Cell Signaling Technology®) and anti-HA antibody (Roche) were used to perform immunoblotting following the manufacturer's instruction.

mtDNA quantification

340 Relative mtDNA was quantified by real-time PCR. Primers based on the cDNA sequences of
341 nuclear-encoded *ACT1* and mitochondrial-encoded *COX1* genes were designed with Primer
342 Express 3.0 (Applied Biosystems, Life Technologies) and purchased from Invitrogen (Life
343 Technologies, sequences available upon request). For each strain analyzed the difference of the
344 threshold cycle number (CT) between *COX1* and *ACT1* (ΔCt) was used to calculate the mtDNA copy
345 number per cell, which was equal to $2^{-\Delta CT}$ [73].
346 *Metabolites analysis*
347 Intracellular metabolites were extracted and analysed by GC-MS. Briefly, around 5 mg of cells in
348 exponential phase of growth (0.7 OD_{600nm}) were harvested by filtration and quenched with 1.5 ml
349 50% MeOH at T<-40 °C, then samples were centrifuged at 13000 rpm for 1 min and supernatant
350 was discarded. To extract metabolites, 400 µl of ice-cold chloroform, 800 µl of 50% MeOH and 20
351 µl of 2 mM norvaline (as internal standard) were added and samples were stirred by vortex for 30
352 min at 4 °C. After 5 min centrifugation at 4 °C, the obtained supernatant was concentrated
353 through evaporation. Samples were subsequently derivatized with MSTFA (N-Methyl-N-
354 (trimethylsilyl) trifluoroacetamide) in an automated WorkBench (Agilent Technologies) and
355 analysed with 7200 accurate-mass Q-TOF GC/MS (Agilent Technologies). Data processing and
356 analysis were performed with Mass Hunter and Mass Profiler Professional software (Agilent
357 Technologies). Raw data were normalized on the norvaline (internal standard) signal and on the
358 collected cell dry weight and reported in Supplementary Table S1.
359 Glucose uptake and glycerol, acetate, pyruvate and ethanol productions were determined by HPLC
360 analysis using a Waters Allianc 2695 separation module (Waters, Milford, MA, USA) equipped with
361 a Rezex ROA-Organic Acid H+ (8%) 300 mm × 7.8 mm column (Phenomenex Inc., USA), coupled to
362 a Waters 2410 refractive index detector and a Waters 2996 UV detector. Separation was carried
363 out at 65 °C with 0.005 M H_2SO_4 as the mobile phase at a flow rate of 0.6 ml/min. The

364 physiological parameters: maximum specific growth rate, biomass yield on glucose and specific
365 glucose consumption rate were calculated during the exponential growth phase, as described [74].
366 Methionine uptake was measured by H-NMR on the medium of exponentially growing cells.
367 Briefly, cells grown in the presence of 0.1 g/L methionine were collected by filtration and
368 resuspended in fresh medium containing 0.1 g/L methionine at a final concentration of 0.1
369 OD_{600nm}. Media were then collected every hour until cells reached the concentration of 1 OD_{600nm}.
370 S-Adenosyl methionine and S-adenosyl homocysteine were measured using the SAM-SAH ELISA kit
371 assay (Cells Biolabs©) following the manufacturer's instructions.
372 *^{13}C-labelling experiments*
373 All labelling experiments were performed in batch cultures assuming pseudo-steady-state
374 conditions during the exponential growth phase in respiro-fermentative conditions [47,75]. ^{13}C-
375 labelling of proteinogenic amino acids was achieved by growth on 20 g/L glucose as a mixture of
376 80% (w/w) unlabelled and 20% (w/w) uniformly labeled [U-^{13}C]glucose (^{13}C, 99 %; Cambridge
377 Isotope Laboratories, Inc). Cells from an overnight minimal medium culture were washed and used
378 for inoculation below an OD_{600} of 0.03. ^{13}C-labelled biomass aliquots were harvested by
379 centrifugation during the mid-exponential growth phase at an OD_{600} of ≤1. Cells (about 0.3 mg of
380 dry biomass) were washed once with sterile water and hydrolysed in 150 µL 6 M HCl at 105 °C for
381 6 h. The hydrolysate was dried in a heating block at 80 °C under a constant airflow. Before the
382 GC/MS analyses all samples were subjected to a derivatization step as follows. Each sample was
383 resuspended in 30 µL of acetonitrile, followed by 30 µL of MBDSTFA (N-methyl-N-ter-
384 butyldimethylsilyl-trifluoroacetamide). The resulting mixture, contained in a closed vial, was
385 stirred for 10 min and centrifuged for 15 sec. Then, the vial was incubated at 85 °C. After 1 h, the
386 sample slowly reached room temperature and was analysed. All the derivatized samples were
387 processed by using a ISQ™ QD Single Quadrupole GC-MS (Thermo Fisher) equipped with a VF-5ms

388 (30 m x 0.25 mm i.d. x 0.25 µm; Agilent Technology). Injection volume: 1 µL. Oven program: 140 °C
389 for 1 min; then 10 °C/min to 310 °C for 1 min; Run Time 15 min. Helium was used as the gas
390 carrier. SS Inlet: Mode Split. Split flow: 15 mL/min. Split ratio: 1/15. Inlet temperature: 270 °C.
391 Flow 1.0 mL/min. MS transfer line: 280 °C. Ion source: 280 °C. Ionization mode: electron impact:
392 70 eV. Acquisition mode: full scan.
393 A METAFOR (metabolic flux ratio) analysis [47] was perfomed on the generated GC-MS data: the
394 mass isotopomer distribution of proteinogenic amino acids was used to calculate the split ratios of
395 key branching points of yeast central metabolism using the software FIAT FLUX [48].
396 *^{13}C-constrained metabolic flux analysis*
397 Intracellular flux ratios , consumption and secretion rates were integrated in a model of yeast
398 central metabolism using the NETTO subprogram of the Fiat Flux software, to obtain network-
399 wide absolute fluxes [47,48].
400 The stoichiometric model for ^{13}C-constrained metabolic flux analysis comprises the major
401 pathways of yeast central carbon metabolism [76]. The model used contains 30 fluxes and 28
402 metabolites. To calculate intracellular fluxes, the stoichiometric model was constrained with five
403 extracellular fluxes (growth rate, glucose uptake rate and production rates of ethanol, glycerol and
404 acetate) and five intracellular flux ratios (fraction of cytosolic oxaloacetate originating from
405 cytosolic pyruvate, fraction of mitochondrial oxaloacetate derived through anaplerosis, fraction of
406 phosphoenol-pyruvate originating from cytosolic oxaloacetate, upper and lower bounds of
407 mitochondrial pyruvate derived through malic enzyme). Only NADH-dependent isocitrate
408 dehydrogenase activity (Idh1 and Idh2) was considered in the model; NADP-specific isocitrate
409 dehydrogenase activity was neglected. Mass balances of O_2, CO_2 and ATP production and
410 consumption were excluded from the analyses. The overly constrained system was solved by a
411 least square optimization as described in [77].

412 *ATP assay*

413 ATP content was quantified using the BacTiter-Glo™ Luminescent Assay (Promega®), following the
414 manufacturer's instructions. Briefly, cells in exponential growth phase were collected and diluted
415 at 0.3 OD_{600nm} and 100 µl of each sample was assayed in triplicate in a 96-well plate. An equal
416 volume of BacTiter-GLO™ was then added to each well and the measurement was carried out
417 after a brief incubation at room temperature (7 min). The measurement was performed at a
418 wavelength of 560 nm with a Cary Eclipse© Luminometer.

419 *Flow cytofluorimetric (FACS) analysis*

420 FACS analysis were performed with the FACSCalibur© Cytofluorimeter and the CellQuest Pro©
421 software as described [27]. Cells were collected at the indicated time points and independently
422 stained with 175 nM 3,3'-dihexyloxacarbocyanine Iodide ($DiOC_6$) to measure mitochondrial
423 potential, with 20 nM Mitotracker green (MTG) to measure the total mitochondrial content. FACS
424 data were analysed with Flowing Software© 2 or with the WinMDI© software which provided
425 quantifications and statistical analysis.

426 *Mitochondrial purification*

427 The isolation of mitochondria was carried out as previously reported [78]. In details, cell walls
428 were enzymatically degraded with Zymolyase. The resulting spheroplasts were disrupted by 13
429 strokes in a cooled Potter-Elvehjem homogenizer in hypotonic medium. Cytosolic and
430 mitochondrial fractions were separated by differential centrifugation. Mitochondria were spun
431 down gently for 10 min at 10,000 x g and were resuspended in a buffer containing 0.6 M mannitol,
432 20 mM Hepes/KOH pH 7.4, 1 mM EGTA, 0.2% bovine serum albumin (BSA) at approximately 10 mg
433 of protein/ml. For the proteomic analysis, mitochondria were further purified using a
434 discontinuous sucrose gradient as described [78].

435 *Proteomic analysis by shotgun mass spectrometry and label free quantification*

436 After reduction and derivatisation [79], the mitochondrial proteins were digested with trypsin
437 sequence grade (Roche) for 16 h at 37 °C using a protein:trypsin ratio of 20:1 [80]. LC-ESI-MS/MS
438 analysis was performed on a Dionex UltiMate 3000 HPLC System with a PicoFrit ProteoPrep C18
439 column (200 mm, internal diameter of 75 µm) (New Objective, USA). Gradient: 1% ACN in 0.1 %
440 formic acid for 10 min, 1-4 % ACN in 0.1% formic acid for 6 min, 4-30% ACN in 0.1% formic acid for
441 147 min and 30-50 % ACN in 0.1% formic for 3 min at a flow rate of 0.3 µl/min. The eluate was
442 electrosprayed into an LTQ Orbitrap Velos (Thermo Fisher Scientific, Bremen, Germany) through a
443 Proxeon nanoelectrospray ion source (Thermo Fisher Scientific) as previously described [81]. Data
444 acquisition was controlled by Xcalibur 2.0 and Tune 2.4 software (Thermo Fisher Scientific). Mass
445 spectra were analysed using MaxQuant software (version 1.3.0.5). The spectra were searched by
446 the Andromeda search engine against the Uniprot sequence database *Saccharomyces cerevisiae*
447 *CEN.PK113-7D* (release 15.12.2016). Protein identification required at least one unique or razor
448 peptide per protein group (FDR 0.01). Quantification in MaxQuant was performed using the built
449 in XIC-based label free quantification (LFQ) algorithm using fast LFQ
450 Statistical analyses were performed using the Perseus software (version 1.5.5.3,
451 www.biochem.mpg.de/mann/tools/). An Anova test (FDR 0.05) was carried out to identify
452 proteins differentially expressed among the different conditions. PCA analysis was performed by
453 Perseus software. Focusing on specific comparison, proteins were considered differentially
454 expressed if they were present only in one condition or showed significant t-test (p value = 0.05).
455 Bioinformatic analyses were carried out by YeastMine software
456 (http://yeastmine.yeastgenome.org) to cluster enriched annotation groups of Biological Processes
457 and Kegg Pathways within the set of identified proteins. Functional grouping was based on p-value
458 ≤0.05 and at least two counts. The mass spectrometry proteomics data have been deposited to

459 the ProteomeXchange Consortium via the PRIDE [82] partner repository with the dataset identifier
460 PXD007644.
461 *Oxygen Consumption*
462 Oxygen consumption by isolated mitochondria was determined at 30 °C using an Oxygraph-2 k
463 system (Oroboros, Innsbruck, Austria) equipped with two chambers in a buffer containing 0.6 M
464 mannitol, 20 mM Hepes/KOH pH 6.8, 10 mM potassium phosphate pH 6.8, 2 mM $MgCl_2$, 1 mM
465 EGTA, and 0.1% BSA. Data was analysed using DatLab software. Measurements were started by
466 adding 1.25 mM NADH or 5 mM succinate, followed by the addition of 0.25 mM ADP.
467 *Statistical analysis*
468 Data are reported as means ± SDs from at least three independent experiments. Statistical
469 significance of the measured differences was assessed by two-tailed Student's t-test (* $p < 0.05$).
470
471
472
473
474

Acknowledgments

This work has been supported by grants to P. Coccetti from the Italian Government (FAR) and to L. Alberghina and P. Coccetti from the SYSBIO, Centre of Systems Biology, a MIUR initiative of the Italian Roadmap of European Strategy Forum on Research Infrastructures (ESFRI). A.C., R.N. and V.R. were supported by fellowships from SYSBIO, while F.T. has been supported by fellowship from MIUR.

We gratefully acknowledge helpful discussion and comments from Dr. Evelina Gatti and Prof. Marco Vanoni.

We kindly thank Prof. Filip Rolland for pYX242-ACC1 and pYX242-ACC1-S79A plasmids.

We thank Prof. Uwe Sauer for FiatFlux software permission and Prof. Lars M. Blank and Dr. Birgitta Ebert for their help with the metabolic flux analysis.

Author contribution

F.T., A.C., V.R., L.L. performed cell biology experiments; F.T., A.C., R.N., C.A, E.F. performed metabolomics experiments; E.M., G.T. performed proteomics experiments and data analysis; G.A., P.S. performed metabolic flux analysis experiments and mitochondria purification; G.T., G.A., L.P., L.A. edited the manuscript; P.C., F.T., G.A. wrote the manuscript and conceived the experiments; P.C. coordinated the project; all the authors read and approved the entire paper.

Competing interest

The authors declare no competing interest.

Table 1. Yeast strains used in this study.

Strain	Genotype	Origin
wt	*CEN.PK JT4 MATα URA3 LEU2 TRP1 HIS3 LCR1*	[49]
snf1Δ	*CEN.PK JT4 MATα URA3 LEU2 TRP1 HIS3 LCR1 snf1::HPH*	This study
mpc1Δ	*CEN.PK JT4 MATα URA3 LEU2 TRP1 HIS3 LCR1 mpc1::NAT1*	This study
mpc1Δ snf1Δ	*CEN.PK JT4 MATα URA3 LEU2 TRP1 HIS3 LCR1 mpc1::NAT1 snf1::HPH*	This study
W303 [ACC1-HA reporter]	*W303-1A leu2-3,112 trp1-1 can1-100 ura3-1 ade2-1 his3-11,15 [pYX242-ACC1-GFP-HA]*	This study
W303 [ACC1-S79A-HA reporter]	*W303-1A leu2-3,112 trp1-1 can1-100 ura3-1 ade2-1 his3-11,15 [pYX242-ACC1-S79A-GFP-HA]*	This study
Mpc1-4HA	*CEN.PK JT4 MATα URA3 LEU2 TRP1 HIS3 LCR1 MPC1-4HA:KANMX4*	This study
Mpc1-4HA snf1Δ	*CEN.PK JT4 MATα URA3 LEU2 TRP1 HIS3 LCR1 snf1::HPH MPC1-4HA:KANMX4*	This study
Mpc2-4HA	*CEN.PK JT4 MATα URA3 LEU2 TRP1 HIS3 LCR1 MPC2-4HA:KANMX4*	This study
Mpc2-4HA snf1Δ	*CEN.PK JT4 MATα URA3 LEU2 TRP1 HIS3 LCR1 snf1::HPH MPC2-4HA:KANMX4*	This study
Mpc3-4HA	*CEN.PK JT4 MATα URA3 LEU2 TRP1 HIS3 LCR1 MPC3-4HA:KANMX4*	This study
Mpc3-4HA snf1Δ	*CEN.PK JT4 MATα URA3 LEU2 TRP1 HIS3 LCR1 snf1::HPH MPC3-4HA:KANMX4*	

Figure legends

Figure 1. Methionine addition impairs the growth rate of the *snf1Δ* mutant.

(A) Snf1 activity was evaluated in wt cells grown with or without 0.1 g/l methionine and expressing the Acc1-pS79 reporter or the non-phosphorylatable Acc1-S79A version. The asterisk indicates a non-specific protein band recognized by the anti-HA antibody, used as loading control. (B) Mass duplication time (MDT) of wt and *snf1Δ* cells grown in the presence of the indicated concentrations of methionine. *p<0.05 (C) Glucose and methionine consumption rate, ethanol, acetate and glycerol secretion rates of wt and *snf1Δ* cells grown in the presence or absence of 0.1 g/l methionine. *p<0.05.

Figure 2. Metabolomic analysis of wt and *snf1Δ* cells grown in the presence or absence of methionine (0.1 g/l).

(A) wt and *snf1Δ* cells were collected in exponential phase and cell lysates were analyzed by GC/MS spectrometry as reported in material and methods. Heat map diagram shows the log2 differential levels of the indicated metabolites. (B) Schematic representation of the methionine cycle in yeast. Solid arrows indicate direct reactions, while dashed arrows indicate reactions with multiple steps. (C) Relative levels of S-adenosylmethionine (SAM) and S-adenosylhomocysteine (SAH) in wt and *snf1Δ* cells. *p<0.05. (D) Ratio between SAM and SAH in wt and *snf1Δ* cells. *p<0.05.

Figure 3. Mitochondrial proteome analysis of wt and *snf1Δ* cells grown in the presence or absence of methionine (0.1 g/l).

(A) Venn diagram of the shotgun proteomic analysis on mitochondria purified from wt and *snf1Δ* cells grown with or without methionine. (B) Principal component analysis of the proteins common among the data sets of wt and *snf1Δ* cells in the presence or absence of 0.1 g/L methionine, whose differences were statistically significant according to ANOVA test (FDR 0.05). (C-F) Biological process enrichment analysis of the proteins differentially expressed between the following pairs of conditions: *snf1Δ vs* wt (C), wt+M *vs* wt (D), *snf1Δ*+M *vs snf1Δ* (E) and *snf1Δ*+M *vs* wt+M (F). For each comparison, BP-enrichment classes with the lowest p-value are shown. For the full lists see Supplementary Tables S3-S6. Bars represent the number of annotated genes in the input list.

Figure 4. Methionine addition stimulates mitochondrial respiration in cells lacking Snf1.

(A) Relative mtDNA copy numbers of wt and *snf1Δ* cells grown in the presence or absence of 0.1 g/l methionine. (B) Ratio between mitochondrial membrane potential and total mitochondrial content of wt and *snf1Δ* cells grown in the presence or absence of 0.1 g/l methionine. Data were obtained by flow cytometric analysis with $DiOC_6$ staining to evaluate the mitochondrial potential

and with Mitotracker Green staining to measure the total mitochondrial content. *p<0.01. (C) Respiration rate of isolated mitochondria from wt and *snf1Δ* cells grown in the presence or absence of 0.1 g/l methionine, in the presence of the indicated oxidizable substrates. *p<0.02. (D) Effect of 1 μg/ml antimycin A on mass duplication time (MDT) of wt and *snf1Δ* cells grown in the presence or absence of 0.1 g/l methionine. * p<0.001. (E) ATP relative level of wt and *snf1Δ* cells grown in the presence or absence of 0.1 g/l methionine. *p<0.005.

Figure 5. Methionine addition enhances mitochondrial pyruvate transport in cells lacking Snf1. (A) Schematic representation of changes in flux through metabolic pathways in *snf1Δ*+M relative to wt+M. (B) Pyruvate transport into mitochondria in wt and *snf1Δ* cells determined by metabolic flux analysis as mmoles of pyruvate per 100 mmoles of glucose taken up by yeast cells. (C) Oxidative TCA cycle activity in wt and *snf1Δ* cells, reported as percentage of mitochondrial oxaloacetate produced from the TCA cycle activity and calculated from ^{13}C-labeling patterns of proteinogenic aminoacids, as described [49].

Figure 6. Cells lacking Snf1 depend on Mpc1 activity. (A) Mpc1,2,3 levels in wt and *snf1Δ* cells expressing HA-tagged versions of the three proteins, grown with or without 0.1 g/l methionine. Anti-Cdc34 antibody was used as loading control. (B) Mass duplication time (MDT) of wt, *snf1Δ* treated with 50 μM UK5099, in the presence or absence of 0.1 g/L methionine. *p<0.05. (C) (B) Mass duplication time (MDT) of wt, *snf1Δ, mpc1Δ* and *mpc1Δsnf1Δ* cells grown in the presence or absence of 0.1 g/L methionine. *p<0.05. (D) Effect of 1 μg/ml antimycin A on mass duplication time (MDT) of *mpc1Δ* and *mpc1Δsnf1Δ* cells grown in the presence or absence of 0.1 g/l methionine.

Figure 7. Relevant connections between Snf1 and methionine metabolism. Schematization of the role of Snf1 and methionine cycle on cellular metabolism. Methionine cycle activates mitochondrial functions and stimulates Snf1/AMPK activity. Snf1/AMPK inhibits glucose uptake

from the medium, pyruvate flux into the mitochondria and respiration. Snf1-dependent function in fine tuning methionine metabolism in a feedback loop is also shown [39].

References

[1] D.G. Hardie, AMP-activated/SNF1 protein kinases: conserved guardians of cellular energy., Nat. Rev. Mol. Cell Biol. 8 (2007) 774–85. doi:10.1038/nrm2249.

[2] D. Thomas, Y. Surdin-Kerjan, Metabolism of sulfur amino acids in Saccharomyces cerevisiae., Microbiol. Mol. Biol. Rev. 61 (1997) 503–32.

[3] K. Hedbacker, M. Carlson, SNF1/AMPK pathways in yeast., Front. Biosci. 13 (2008) 2408–20. doi:10.2741/2854.

[4] M.C. Schmidt, R.R. McCartney, beta-subunits of Snf1 kinase are required for kinase function and substrate definition., EMBO J. 19 (2000) 4936–43. doi:10.1093/emboj/19.18.4936.

[5] R.R. McCartney, M.C. Schmidt, Regulation of Snf1 Kinase. Activation requires phosphorylation of threonine 210 by an upstream kinase as well as a distinct step mediated by the Snf4 subunit, J. Biol. Chem. 276 (2001) 36460–36466. doi:10.1074/jbc.M104418200.

[6] J. Tu, M. Carlson, REG1 binds to protein phosphatase type 1 and regulates glucose repression in Saccharomyces cerevisiae., EMBO J. 14 (1995) 5939–46. http://www.pubmedcentral.nih.gov/articlerender.fcgi?artid=394713&tool=pmcentrez&rendertype=abstract (accessed February 17, 2011).

[7] Y. Zhang, R.R. McCartney, D.G. Chandrashekarappa, S. Mangat, M.C. Schmidt, Reg1 Protein Regulates Phosphorylation of All Three Snf1 Isoforms but Preferentially Associates with the Gal83 Isoform, Eukaryot. Cell. 10 (2011) 1628–1636. doi:10.1128/EC.05176-11.

[8] R.R. McCartney, L. Garnar-Wortzel, D.G. Chandrashekarappa, M.C. Schmidt, Activation and inhibition of Snf1 kinase activity by phosphorylation within the activation loop, Biochim. Biophys. Acta - Proteins Proteomics. 1864 (2016) 1518–1528.

582 doi:10.1016/j.bbapap.2016.08.007.
583 [9] M.J. DeVit, M. Johnston, The nuclear exportin Msn5 is required for nuclear export of the
584 Mig1 glucose repressor of Saccharomyces cerevisiae., Curr. Biol. 9 (1999) 1231–1241.
585 doi:10.1016/S0960-9822(99)80503-X.
586 [10] F.C. Smith, S.P. Davies, W.A. Wilson, D. Carling, D.G. Hardie, The SNF1 kinase complex from
587 *Saccharomyces cerevisiae* phosphorylates the transcriptional repressor protein Mig1p in
588 vitro at four sites within or near regulatory domain 1, FEBS Lett. 453 (1999) 219–223.
589 doi:10.1016/S0014-5793(99)00725-5.
590 [11] D. Hedges, M. Proft, K.D. Entian, CAT8, a new zinc cluster-encoding gene necessary for
591 derepression of gluconeogenic enzymes in the yeast Saccharomyces cerevisiae., Mol. Cell.
592 Biol. 15 (1995) 1915–22. doi:10.1128/MCB.15.4.1915.
593 [12] F. Randez-Gil, N. Bojunga, M. Proft, K.D. Entian, Glucose derepression of gluconeogenic
594 enzymes in Saccharomyces cerevisiae correlates with phosphorylation of the gene activator
595 Cat8p., Mol. Cell. Biol. 17 (1997) 2502–10. doi:10.1128/MCB.17.5.2502.
596 [13] E.T. Young, K.M. Dombek, C. Tachibana, T. Ideker, Multiple pathways are co-regulated by
597 the protein kinase Snf1 and the transcription factors Adr1 and Cat8., J. Biol. Chem. 278
598 (2003) 26146–58. doi:10.1074/jbc.M301981200.
599 [14] E.T. Young, N. Kacherovsky, K. Van Riper, Snf1 protein kinase regulates Adr1 binding to
600 chromatin but not transcription activation., J. Biol. Chem. 277 (2002) 38095–103.
601 doi:10.1074/jbc.M206158200.
602 [15] M.J. Rodríguez-Colman, M.A. Sorolla, N. Vall-llaura, J. Tamarit, J. Ros, E. Cabiscol, The FOX
603 transcription factor Hcm1 regulates oxidative metabolism in response to early nutrient
604 limitation in yeast. Role of Snf1 and Tor1/Sch9 kinases, Biochim. Biophys. Acta - Mol. Cell
605 Res. 1833 (2013) 2004–2015. doi:10.1016/j.bbamcr.2013.02.015.

606 [16] Y.J. Lee, G.R. Jeschke, F.M. Roelants, J. Thorner, B.E. Turk, Reciprocal phosphorylation of
607 yeast glycerol-3-phosphate dehydrogenases in adaptation to distinct types of stress., Mol.
608 Cell. Biol. 32 (2012) 4705–17. doi:10.1128/MCB.00897-12.
609 [17] M.K. Shirra, J. Patton-Vogt, A. Ulrich, O. Liuta-Tehlivets, S.D. Kohlwein, S.A. Henry, K.M.
610 Arndt, Inhibition of acetyl coenzyme A carboxylase activity restores expression of the INO1
611 gene in a snf1 mutant strain of Saccharomyces cerevisiae., Mol. Cell. Biol. 21 (2001) 5710–
612 22. doi:10.1128/MCB.21.17.5710-5722.2001.
613 [18] S. Shi, Y. Chen, V. Siewers, J. Nielsen, Improving production of malonyl coenzyme A-derived
614 metabolites by abolishing Snf1-dependent regulation of Acc1., MBio. 5 (2014) e01130-14.
615 doi:10.1128/mBio.01130-14.
616 [19] M.K. Shirra, R.R. McCartney, C. Zhang, K.M. Shokat, M.C. Schmidt, K.M. Arndt, A chemical
617 genomics study identifies Snf1 as a repressor of GCN4 translation., J. Biol. Chem. 283 (2008)
618 35889–98. doi:10.1074/jbc.M805325200.
619 [20] R. Usaite, M.C. Jewett, A.P. Oliveira, J.R. Yates, L. Olsson, J. Nielsen, Reconstruction of the
620 yeast Snf1 kinase regulatory network reveals its role as a global energy regulator., Mol. Syst.
621 Biol. 5 (2009) 319. doi:10.1038/msb.2009.67.
622 [21] J. Zhang, S. Vaga, P. Chumnanpuen, R. Kumar, G.N. Vemuri, R. Aebersold, J. Nielsen,
623 Mapping the interaction of Snf1 with TORC1 in Saccharomyces cerevisiae., Mol. Syst. Biol. 7
624 (2011) 545. doi:10.1038/msb.2011.80.
625 [22] D. Ahuatzi, A. Riera, R. Peláez, P. Herrero, F. Moreno, Hxk2 regulates the phosphorylation
626 state of Mig1 and therefore its nucleocytoplasmic distribution., J. Biol. Chem. 282 (2007)
627 4485–93. doi:10.1074/jbc.M606854200.
628 [23] A.F. O'Donnell, R.R. McCartney, D.G. Chandrashekarappa, B.B. Zhang, J. Thorner, M.C.
629 Schmidt, 2-Deoxyglucose impairs Saccharomyces cerevisiae growth by stimulating Snf1-

630 regulated and α-arrestin-mediated trafficking of hexose transporters 1 and 3., Mol. Cell.
631 Biol. 35 (2015) 939–55. doi:10.1128/MCB.01183-14.
632 [24] F. Galello, C. Pautasso, S. Reca, L. Cañonero, P. Portela, S. Moreno, S. Rossi, Transcriptional
633 regulation of the protein kinase a subunits in Saccharomyces cerevisiae during fermentative
634 growth., Yeast. 34 (2017) 495–508. doi:10.1002/yea.3252.
635 [25] S. Busnelli, F. Tripodi, R. Nicastro, C. Cirulli, G. Tedeschi, R. Pagliarin, L. Alberghina, P.
636 Coccetti, Snf1/AMPK promotes SBF and MBF-dependent transcription in budding yeast.,
637 Biochim. Biophys. Acta. 1833 (2013) 3254–64. doi:10.1016/j.bbamcr.2013.09.014.
638 [26] R. Nicastro, F. Tripodi, C. Guzzi, V. Reghellin, S. Khoomrung, C. Capusoni, C. Compagno, C.
639 Airoldi, J. Nielsen, L. Alberghina, P. Coccetti, Enhanced amino acid utilization sustains
640 growth of cells lacking Snf1/AMPK, Biochim. Biophys. Acta - Mol. Cell Res. 1853 (2015)
641 1615–1625. doi:10.1016/j.bbamcr.2015.03.014.
642 [27] S. Pessina, V. Tsiarentsyeva, S. Busnelli, M. Vanoni, L. Alberghina, P. Coccetti, Snf1/AMPK
643 promotes S-phase entrance by controlling CLB5 transcription in budding yeast., Cell Cycle. 9
644 (2010) 2189–200. doi:10.4161/cc.9.11.11847.
645 [28] F. Tripodi, R. Fraschini, M. Zocchi, V. Reghellin, P. Coccetti, Snf1/AMPK is involved in the
646 mitotic spindle alignment in Saccharomyces cerevisiae, Sci. Rep. 8 (2018) 5853.
647 doi:10.1038/s41598-018-24252-y.
648 [29] R. Nicastro, F. Tripodi, M. Gaggini, A. Castoldi, V. Reghellin, S. Nonnis, G. Tedeschi, P.
649 Coccetti, Snf1 phosphorylates adenylate cyclase and negatively regulates protein kinase A-
650 dependent transcription in Saccharomyces cerevisiae, J. Biol. Chem. 290 (2015) 24715–
651 24726. doi:10.1074/jbc.M115.658005.
652 [30] P.K. Chiang, R.K. Gordon, J. Tal, G.C. Zeng, B.P. Doctor, K. Pardhasaradhi, P.P. McCann, S-
653 Adenosylmethionine and methylation., FASEB J. 10 (1996) 471–80.

[31] S.J. Mentch, J.W. Locasale, One-carbon metabolism and epigenetics: understanding the specificity., Ann. N. Y. Acad. Sci. 1363 (2016) 91–8. doi:10.1111/nyas.12956.

[32] D.E. Vance, Phospholipid methylation in mammals: from biochemistry to physiological function, Biochim. Biophys. Acta - Biomembr. 1838 (2014) 1477–1487. doi:10.1016/j.bbamem.2013.10.018.

[33] R.S. McIsaac, K.N. Lewis, P.A. Gibney, R. Buffenstein, From yeast to human: exploring the comparative biology of methionine restriction in extending eukaryotic life span, Ann. N. Y. Acad. Sci. 1363 (2016) 155–170. doi:10.1111/nyas.13032.

[34] R. Murín, E. Vidomanová, B.S. Kowtharapu, J. Hatok, D. Dobrota, Role of S-adenosylmethionine cycle in carcinogenesis, Gen. Physiol. Biophys. 36 (2017) 513–520. doi:10.4149/gpb_2017031.

[35] S. Tang, Y. Fang, G. Huang, X. Xu, E. Padilla-Banks, W. Fan, Q. Xu, S.M. Sanderson, J.F. Foley, S. Dowdy, M.W. McBurney, D.C. Fargo, C.J. Williams, J.W. Locasale, Z. Guan, X. Li, Methionine metabolism is essential for SIRT1-regulated mouse embryonic stem cell maintenance and embryonic development., EMBO J. 36 (2017) 3175–3193. doi:10.15252/embj.201796708.

[36] G.P. Ables, J.E. Johnson, Pleiotropic responses to methionine restriction., Exp. Gerontol. 94 (2017) 83–88. doi:10.1016/j.exger.2017.01.012.

[37] R. Koziel, C. Ruckenstuhl, E. Albertini, M. Neuhaus, C. Netzberger, M. Bust, F. Madeo, R.J. Wiesner, P. Jansen-D??rr, Methionine restriction slows down senescence in human diploid fibroblasts, Aging Cell. 13 (2014) 1038–1048. doi:10.1111/acel.12266.

[38] M. Mizunuma, K. Miyamura, D. Hirata, H. Yokoyama, T. Miyakawa, Involvement of S-adenosylmethionine in G1 cell-cycle regulation in Saccharomyces cerevisiae., Proc. Natl. Acad. Sci. U. S. A. 101 (2004) 6086–91. doi:10.1073/pnas.0308314101.

[39] T. Ogawa, R. Tsubakiyama, M. Kanai, T. Koyama, T. Fujii, H. Iefuji, T. Soga, K. Kume, T. Miyakawa, D. Hirata, M. Mizunuma, Stimulating S-adenosyl-l-methionine synthesis extends lifespan via activation of AMPK., Proc. Natl. Acad. Sci. U. S. A. 113 (2016) 11913–11918. doi:10.1073/pnas.1604047113.

[40] S. Deroover, R. Ghillebert, T. Broeckx, J. Winderickx, F. Rolland, Trehalose-6-phosphate synthesis controls yeast gluconeogenesis downstream and independent of SNF1, FEMS Yeast Res. 16 (2016) fow036. doi:10.1093/femsyr/fow036.

[41] S. Sengupta, P. Chaudhuri, S. Lahiri, T. Dutta, S. Banerjee, R. Majhi, A.K. Ghosh, Possible regulation of trehalose metabolism by methylation in Saccharomyces cerevisiae, J. Cell. Physiol. 226 (2011) 158–164. doi:10.1002/jcp.22317.

[42] M. Morgenstern, S.B. Stiller, P. Lübbert, C.D. Peikert, S. Dannenmaier, F. Drepper, U. Weill, P. Höß, R. Feuerstein, M. Gebert, M. Bohnert, M. van der Laan, M. Schuldiner, C. Schütze, S. Oeljeklaus, N. Pfanner, N. Wiedemann, B. Warscheid, Definition of a High-Confidence Mitochondrial Proteome at Quantitative Scale., Cell Rep. 19 (2017) 2836–2852. doi:10.1016/j.celrep.2017.06.014.

[43] V. Strogolova, M. Orlova, A. Shevade, S. Kuchin, Mitochondrial Porin Por1 and Its Homolog Por2 Contribute to the Positive Control of Snf1 Protein Kinase in Saccharomyces cerevisiae, Eukaryot. Cell. 11 (2012) 1568–1572. doi:10.1128/EC.00127-12.

[44] T. Izawa, S.-H. Park, L. Zhao, F.U. Hartl, W. Neupert, Cytosolic Protein Vms1 Links Ribosome Quality Control to Mitochondrial and Cellular Homeostasis, Cell. 171 (2017) 890–903.e18. doi:10.1016/j.cell.2017.10.002.

[45] A. Alexandre, A.L. Lehninger, Bypasses of the antimycin A block of mitochondrial electron transport in relation to ubisemiquinone function, Biochim. Biophys. Acta - Bioenerg. 767 (1984) 120–129. doi:10.1016/0005-2728(84)90086-0.

[46] M.L. Campo, K.W. Kinnally, H. Tedeschi, The effect of antimycin A on mouse liver inner mitochondrial membrane channel activity., J. Biol. Chem. 267 (1992) 8123–7.

[47] L.M. Blank, U. Sauer, TCA cycle activity in Saccharomyces cerevisiae is a function of the environmentally determined specific growth and glucose uptake rates, Microbiology. 150 (2004) 1085–1093. doi:10.1099/mic.0.26845-0.

[48] N. Zamboni, E. Fischer, U. Sauer, FiatFlux--a software for metabolic flux analysis from 13C-glucose experiments., BMC Bioinformatics. 6 (2005) 209. doi:10.1186/1471-2105-6-209.

[49] A. Kümmel, J.C. Ewald, S.-M. Fendt, S.J. Jol, P. Picotti, R. Aebersold, U. Sauer, N. Zamboni, M. Heinemann, D. Ahuatzi, P. Herrero, T.D. La Cera, F. Moreno, D. Ahuatzi, A. Riera, R. Pelaez, P. Herrero, F. Moreno, L. Beney, P. Marechal, P. Gervais, L. Bisson, V. Kunathigan, L. Blank, U. Sauer, E. Boyle, S. Weng, J. Gollub, H. Jin, D. Botstein, J. Cherry, G. Sherlock, C. Brachmann, A. Davies, G. Cost, E. Caputo, J. Li, P. Hieter, J. Boeke, M. Carlson, W. De Koning, K. Van Dam, T.D. La Cera, P. Herrero, F. Moreno-Herrero, R. Chaves, F. Moreno, J. De Winde, M. Crauwels, S. Hohmann, J. Thevelein, J. Winderickx, K. Elbing, C. Larsson, R. Bill, K. Entian, P. Eraso, J. Gancedo, J. Ewald, S. Heux, N. Zamboni, E. Fischer, N. Zamboni, U. Sauer, J. Gancedo, B. Gonzalez, J. Francois, M. Renaud, W. Gorner, E. Durchschlag, M. Martinez-Pastor, U. Guldener, S. Heck, T. Fielder, J. Beinhauer, J. Hegemann, V. Haurie, F. Sagliocco, H. Boucherie, K. Hedbacker, R. Townley, M. Carlson, J. Horak, J. Regelmann, D. Wolf, H. Jiang, I. Medintz, B. Zhang, C. Michels, M. Johnston, J. Kim, N. King, E. Deutsch, J. Ranish, A. Kümmel, S. Panke, M. Heinemann, V. Lange, J. Malmstrom, J. Didion, B. Luo, K. Groenke, R. Takors, C. Wandrey, M. Oldiges, H. Ma, D. Botstein, P. Mallick, M. Schirle, S. Chen, M. Martinez-Pastor, G. Marchler, C. Schuller, A. Marchler-Bauer, H. Ruis, F. Estruch, K. Mbonyi, L. Van Aelst, J. Arguelles, A. Jans, J. Thevelein, J. Navarro-Avino, R. Prasad, V. Miralles, R. Benito, R. Serrano, K. Otterstedt, C. Larsson, R. Bill, A. Stahlberg, E. Boles, S. Hohmann, L.

Gustafsson, P. Picotti, H. Lam, D. Campbell, F. Randez-Gil, P. Sanz, K. Entian, J. Prieto, A. Rodriguez, T.D. La Cera, P. Herrero, F. Moreno, F. Rolland, J. Winderickx, J. Thevelein, M. Rose, W. Albig, K. Entian, G. Santangelo, J. Schacherer, D. Ruderfer, D. Gresham, K. Dolinski, D. Botstein, L. Kruglyak, J. Schuurmans, A. Boorsma, R. Lascaris, K. Hellingwerf, M.T. de Mattos, M. Slattery, D. Liko, W. Heideman, M. Teixeira, P. Monteiro, P. Jain, H. Tettelin, M.A. Carbone, K. Albermann, J. Thevelein, J. De Winde, S. Thompson-Jaeger, J. Francois, J. Gaughran, K. Tatchell, J. Van Dijken, J. Bauer, L. Brambilla, M. Vanhalewyn, F. Dumortier, G. Debast, C. Verduyn, E. Postma, W. Scheffers, J. Van Dijken, S. Westergaard, A. Oliveira, C. Bro, L. Olsson, J. Nielsen, F. Winston, C. Dollard, S. Ricupero-Hovasse, N. Zamboni, E. Fischer, U. Sauer, O. Zaragoza, C. Lindley, J. Gancedo, F. Zimmermann, I. Scheel, Differential glucose repression in common yeast strains in response to HXK2 deletion., FEMS Yeast Res. 10 (2010) 322–32. doi:10.1111/j.1567-1364.2010.00609.x.

[50] J.C.W. Hildyard, C. Ammälä, I.D. Dukes, S.A. Thomson, A.P. Halestrap, Identification and characterisation of a new class of highly specific and potent inhibitors of the mitochondrial pyruvate carrier., Biochim. Biophys. Acta. 1707 (2005) 221–30. doi:10.1016/j.bbabio.2004.12.005.

[51] S. Herzig, E. Raemy, S. Montessuit, J.-L. Veuthey, N. Zamboni, B. Westermann, E.R.S. Kunji, J.-C. Martinou, Identification and Functional Expression of the Mitochondrial Pyruvate Carrier, Science (80-.). 337 (2012) 93–96. doi:10.1126/science.1218530.

[52] D.K. Bricker, E.B. Taylor, J.C. Schell, T. Orsak, A. Boutron, Y.-C. Chen, J.E. Cox, C.M. Cardon, J.G. Van Vranken, N. Dephoure, C. Redin, S. Boudina, S.P. Gygi, M. Brivet, C.S. Thummel, J. Rutter, A Mitochondrial Pyruvate Carrier Required for Pyruvate Uptake in Yeast, Drosophila, and Humans, Science (80-.). 337 (2012) 96–100. doi:10.1126/science.1218099.

[53] M. Kanai, M. Masuda, Y. Takaoka, H. Ikeda, K. Masaki, T. Fujii, H. Iefuji, Adenosine kinase-

750 deficient mutant of Saccharomyces cerevisiae accumulates S-adenosylmethionine because
751 of an enhanced methionine biosynthesis pathway., Appl. Microbiol. Biotechnol. 97 (2013)
752 1183–90. doi:10.1007/s00253-012-4261-3.
753 [54] O. Tehlivets, N. Malanovic, M. Visram, T. Pavkov-Keller, W. Keller, S-adenosyl-L-
754 homocysteine hydrolase and methylation disorders: yeast as a model system., Biochim.
755 Biophys. Acta. 1832 (2013) 204–15. doi:10.1016/j.bbadis.2012.09.007.
756 [55] M. Shobayashi, N. Mukai, K. Iwashita, Y. Hiraga, H. Iefuji, A new method for isolation of S-
757 adenosylmethionine (SAM)-accumulating yeast., Appl. Microbiol. Biotechnol. 69 (2006)
758 704–10. doi:10.1007/s00253-005-0009-7.
759 [56] K. Hayakawa, S. Kajihata, F. Matsuda, H. Shimizu, 13C-metabolic flux analysis in S-adenosyl-
760 l-methionine production by Saccharomyces cerevisiae, J. Biosci. Bioeng. 120 (2015) 532–
761 538. doi:10.1016/j.jbiosc.2015.03.010.
762 [57] J. Feng, S. Lü, Y. Ding, M. Zheng, X. Wang, Homocysteine activates T cells by enhancing
763 endoplasmic reticulum-mitochondria coupling and increasing mitochondrial respiration.,
764 Protein Cell. 7 (2016) 391–402. doi:10.1007/s13238-016-0245-x.
765 [58] A. Kumar, L. John, S. Maity, M. Manchanda, A. Sharma, N. Saini, K. Chakraborty, S.
766 Sengupta, Converging evidence of mitochondrial dysfunction in a yeast model of
767 homocysteine metabolism imbalance., J. Biol. Chem. 286 (2011) 21779–95.
768 doi:10.1074/jbc.M111.228072.
769 [59] T. Bender, J.-C. Martinou, The mitochondrial pyruvate carrier in health and disease: To carry
770 or not to carry?, Biochim. Biophys. Acta. 1863 (2016) 2436–42.
771 doi:10.1016/j.bbamcr.2016.01.017.
772 [60] A. Martínez-Zamora, S. Meseguer, J.M. Esteve, M. Villarroya, C. Aguado, J.A. Enríquez, E.
773 Knecht, M.-E. Armengod, Defective Expression of the Mitochondrial-tRNA Modifying

774 Enzyme GTPBP3 Triggers AMPK-Mediated Adaptive Responses Involving Complex I
775 Assembly Factors, Uncoupling Protein 2, and the Mitochondrial Pyruvate Carrier., PLoS One.
776 10 (2015) e0144273. doi:10.1371/journal.pone.0144273.
777 [61] J.C. Schell, K.A. Olson, L. Jiang, A.J. Hawkins, J.G. Van Vranken, J. Xie, R.A. Egnatchik, E.G.
778 Earl, R.J. DeBerardinis, J. Rutter, A role for the mitochondrial pyruvate carrier as a repressor
779 of the Warburg effect and colon cancer cell growth., Mol. Cell. 56 (2014) 400–13.
780 doi:10.1016/j.molcel.2014.09.026.
781 [62] X. Li, G. Han, X. Li, Q. Kan, Z. Fan, Y. Li, Y. Ji, J. Zhao, M. Zhang, M. Grigalavicius, V. Berge,
782 M.A. Goscinski, J.M. Nesland, Z. Suo, Mitochondrial pyruvate carrier function determines
783 cell stemness and metabolic reprogramming in cancer cells, Oncotarget. 8 (2017) 46363–
784 46380. doi:10.18632/oncotarget.18199.
785 [63] C. Yang, B. Ko, C.T. Hensley, L. Jiang, A.T. Wasti, J. Kim, J. Sudderth, M.A. Calvaruso, L.
786 Lumata, M. Mitsche, J. Rutter, M.E. Merritt, R.J. DeBerardinis, Glutamine Oxidation
787 Maintains the TCA Cycle and Cell Survival during Impaired Mitochondrial Pyruvate
788 Transport, Mol. Cell. 56 (2014) 414–424. doi:10.1016/j.molcel.2014.09.025.
789 [64] F. Weinberg, R. Hamanaka, W.W. Wheaton, S. Weinberg, J. Joseph, M. Lopez, B.
790 Kalyanaraman, G.M. Mutlu, G.R.S. Budinger, N.S. Chandel, Mitochondrial metabolism and
791 ROS generation are essential for Kras-mediated tumorigenicity., Proc. Natl. Acad. Sci. U. S.
792 A. 107 (2010) 8788–93. doi:10.1073/pnas.1003428107.
793 [65] K. Smolková, L. Plecitá-Hlavatá, N. Bellance, G. Benard, R. Rossignol, P. Ježek, Waves of gene
794 regulation suppress and then restore oxidative phosphorylation in cancer cells., Int. J.
795 Biochem. Cell Biol. 43 (2011) 950–68. doi:10.1016/j.biocel.2010.05.003.
796 [66] B. Faubert, G. Boily, S. Izreig, T. Griss, B. Samborska, Z. Dong, F. Dupuy, C. Chambers, B.J.
797 Fuerth, B. Viollet, O.A. Mamer, D. Avizonis, R.J. DeBerardinis, P.M. Siegel, R.G. Jones, AMPK

798 is a negative regulator of the Warburg effect and suppresses tumor growth in vivo., Cell
799 Metab. 17 (2013) 113–24. doi:10.1016/j.cmet.2012.12.001.
800 [67] I. Papandreou, A.L. Lim, K. Laderoute, N.C. Denko, Hypoxia signals autophagy in tumor cells
801 via AMPK activity, independent of HIF-1, BNIP3, and BNIP3L., Cell Death Differ. 15 (2008)
802 1572–81. doi:10.1038/cdd.2008.84.
803 [68] K.E. Matlack, B. Misselwitz, K. Plath, T.A. Rapoport, BiP acts as a molecular ratchet during
804 posttranslational transport of prepro-alpha factor across the ER membrane., Cell. 97 (1999)
805 553–64. http://www.ncbi.nlm.nih.gov/pubmed/10367885 (accessed February 21, 2018).
806 [69] Y. Kimura, K. Irie, T. Mizuno, Expression control of the AMPK regulatory subunit and its
807 functional significance in yeast ER stress response, Sci. Rep. 7 (2017) 46713.
808 doi:10.1038/srep46713.
809 [70] T. Mizuno, Y. Masuda, K. Irie, The Saccharomyces cerevisiae AMPK, Snf1, Negatively
810 Regulates the Hog1 MAPK Pathway in ER Stress Response, PLOS Genet. 11 (2015) e1005491.
811 doi:10.1371/journal.pgen.1005491.
812 [71] J. Ferrer-Dalmau, F. Randez-Gil, M. Marquina, J.A. Prieto, A. Casamayor, Protein kinase Snf1
813 is involved in the proper regulation of the unfolded protein response in Saccharomyces
814 cerevisiae., Biochem. J. 468 (2015) 33–47. doi:10.1042/BJ20140734.
815 [72] M. Zhang, L. Galdieri, A. Vancura, The yeast AMPK homolog SNF1 regulates acetyl coenzyme
816 A homeostasis and histone acetylation., Mol. Cell. Biol. 33 (2013) 4701–17.
817 doi:10.1128/MCB.00198-13.
818 [73] J.P. Rooney, I.T. Ryde, L.H. Sanders, E.H. Howlett, M.D. Colton, K.E. Germ, G.D. Mayer, J.T.
819 Greenamyre, J.N. Meyer, PCR based determination of mitochondrial DNA copy number in
820 multiple species., Methods Mol. Biol. 1241 (2015) 23–38. doi:10.1007/978-1-4939-1875-
821 1_3.

[74] G. Agrimi, M.C. Mena, K. Izumi, I. Pisano, L. Germinario, H. Fukuzaki, L. Palmieri, L.M. Blank, H. Kitagaki, Improved sake metabolic profile during fermentation due to increased mitochondrial pyruvate dissimilation., FEMS Yeast Res. 14 (2014) 249–60. doi:10.1111/1567-1364.12120.

[75] E. Fischer, U. Sauer, Metabolic flux profiling of Escherichia coli mutants in central carbon metabolism using GC-MS., Eur. J. Biochem. 270 (2003) 880–91. http://www.ncbi.nlm.nih.gov/pubmed/12603321 (accessed February 14, 2018).

[76] J. Heyland, J. Fu, L.M. Blank, Correlation between TCA cycle flux and glucose uptake rate during respiro-fermentative growth of Saccharomyces cerevisiae., Microbiology. 155 (2009) 3827–37. doi:10.1099/mic.0.030213-0.

[77] E. Fischer, N. Zamboni, U. Sauer, High-throughput metabolic flux analysis based on gas chromatography-mass spectrometry derived 13C constraints., Anal. Biochem. 325 (2004) 308–16. http://www.ncbi.nlm.nih.gov/pubmed/14751266 (accessed February 14, 2018).

[78] C. Meisinger, T. Sommer, N. Pfanner, Purification of Saccharomcyes cerevisiae mitochondria devoid of microsomal and cytosolic contaminations., Anal. Biochem. 287 (2000) 339–42. doi:10.1006/abio.2000.4868.

[79] E. Toffolo, F. Rusconi, L. Paganini, M. Tortorici, S. Pilotto, C. Heise, C. Verpelli, G. Tedeschi, E. Maffioli, C. Sala, A. Mattevi, E. Battaglioli, Phosphorylation of neuronal Lysine-Specific Demethylase 1LSD1/KDM1A impairs transcriptional repression by regulating interaction with CoREST and histone deacetylases HDAC1/2., J. Neurochem. 128 (2014) 603–16. doi:10.1111/jnc.12457.

[80] P. Coccetti, F. Tripodi, G. Tedeschi, S. Nonnis, O. Marin, S. Fantinato, C. Cirulli, M. Vanoni, L. Alberghina, The CK2 phosphorylation of catalytic domain of Cdc34 modulates its activity at the G1 to S transition in Saccharomyces cerevisiae, Cell Cycle. 7 (2008) 1391–1401.

[81] E. Maffioli, S. Nonnis, R. Angioni, F. Santagata, B. Calì, L. Zanotti, A. Negri, A. Viola, G. Tedeschi, Proteomic analysis of the secretome of human bone marrow-derived mesenchymal stem cells primed by pro-inflammatory cytokines., J. Proteomics. 166 (2017) 115–126. doi:10.1016/j.jprot.2017.07.012.

[82] J.A. Vizcaíno, A. Csordas, N. del-Toro, J.A. Dianes, J. Griss, I. Lavidas, G. Mayer, Y. Perez-Riverol, F. Reisinger, T. Ternent, Q.-W. Xu, R. Wang, H. Hermjakob, 2016 update of the PRIDE database and its related tools, Nucleic Acids Res. 44 (2016) D447–D456. doi:10.1093/nar/gkv1145.

Figure1

Click here to download high resolution image

Figure 1

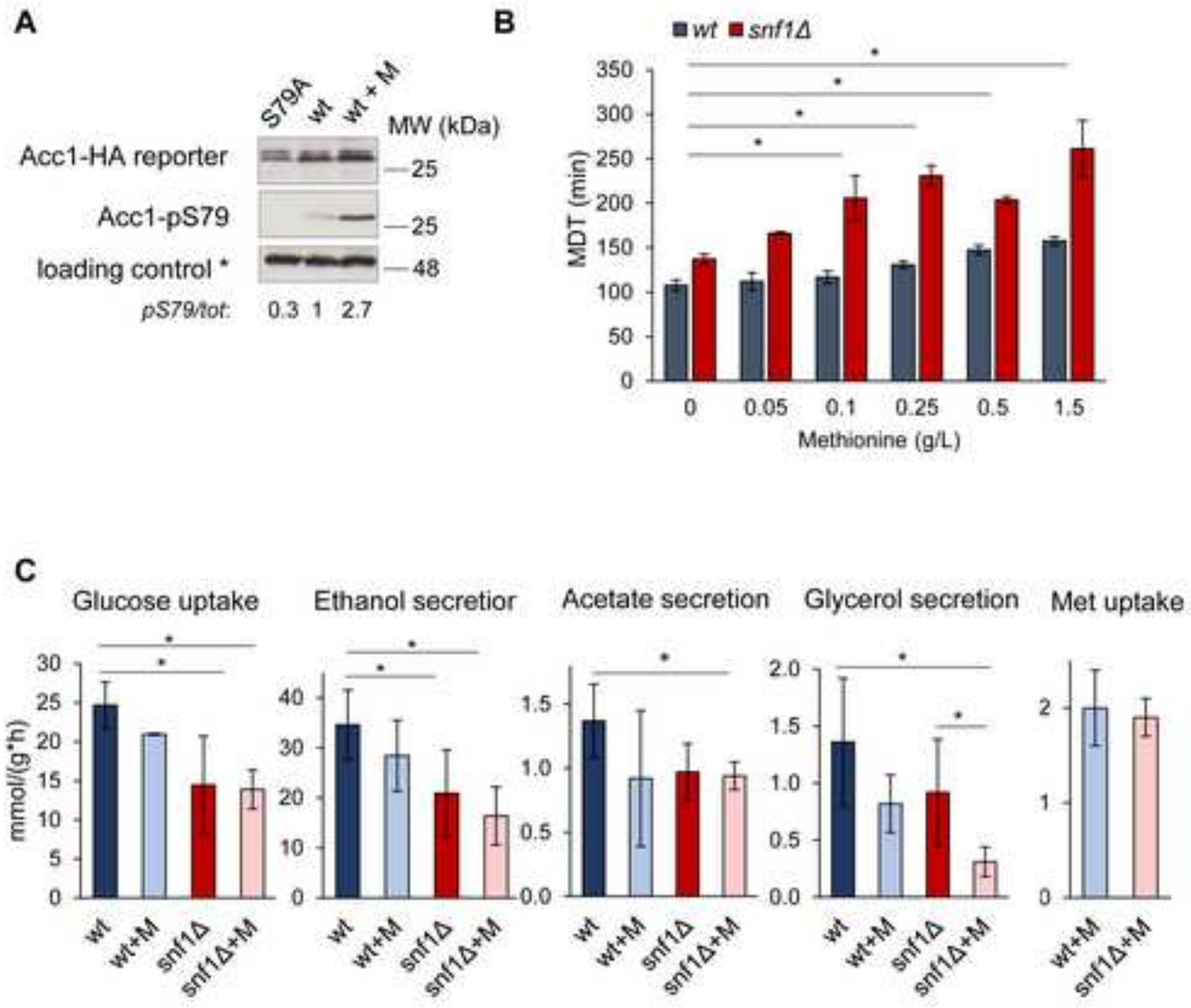

Figure2

Click here to download high resolution image

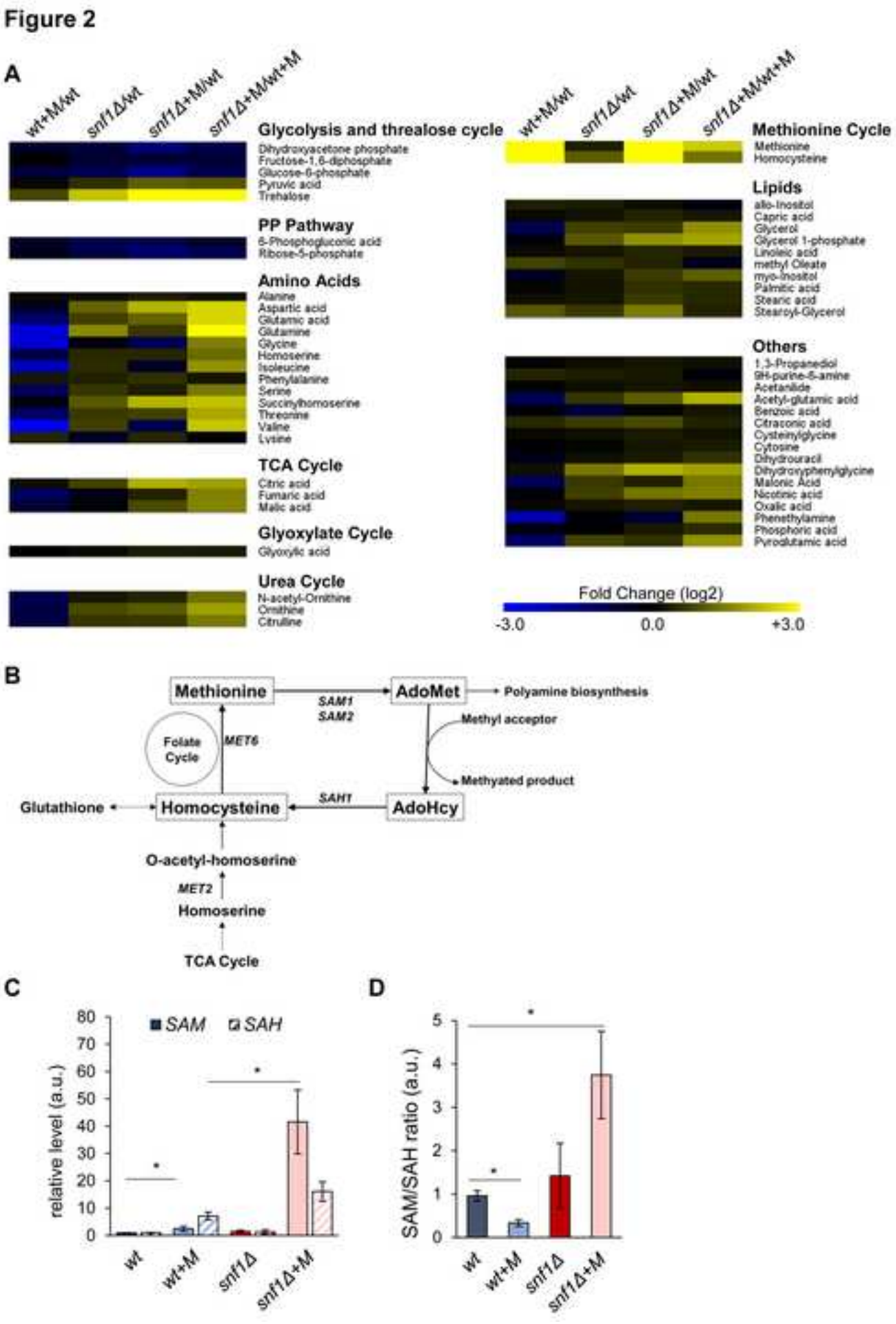

Figure3 part1

Click here to download high resolution image

Figure 3

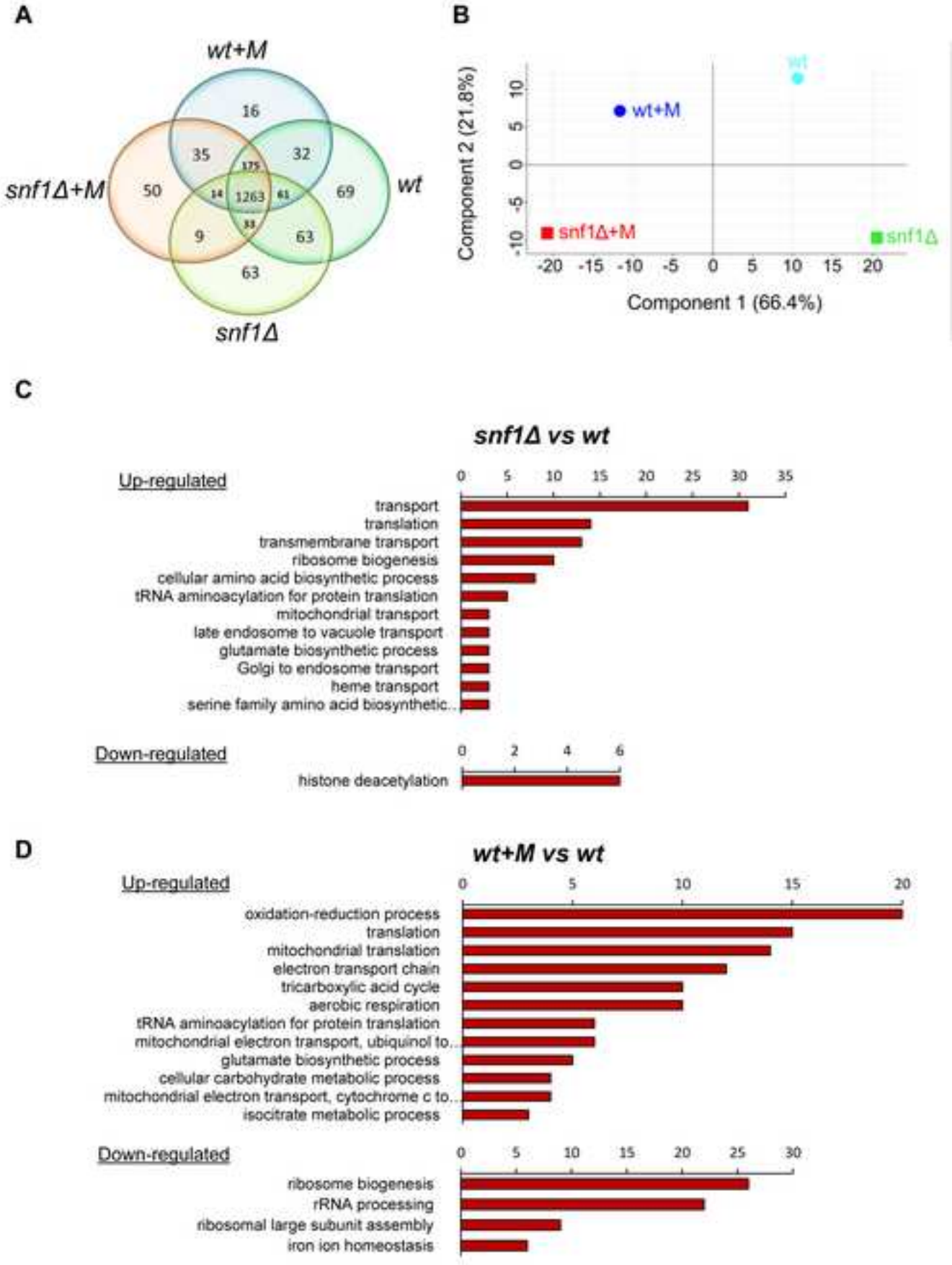

Figure3 part2

Click here to download high resolution image

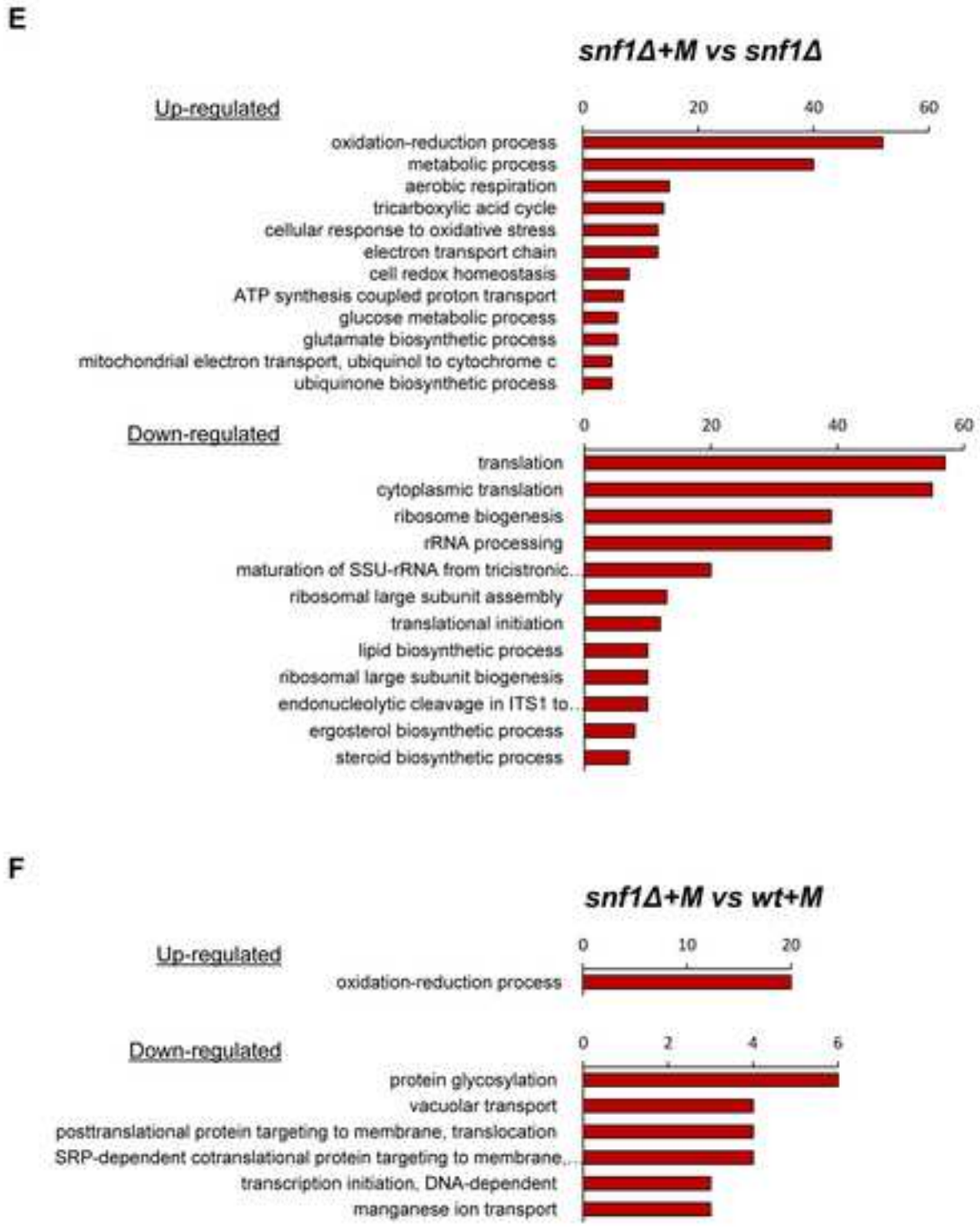

Figure4

Click here to download high resolution image

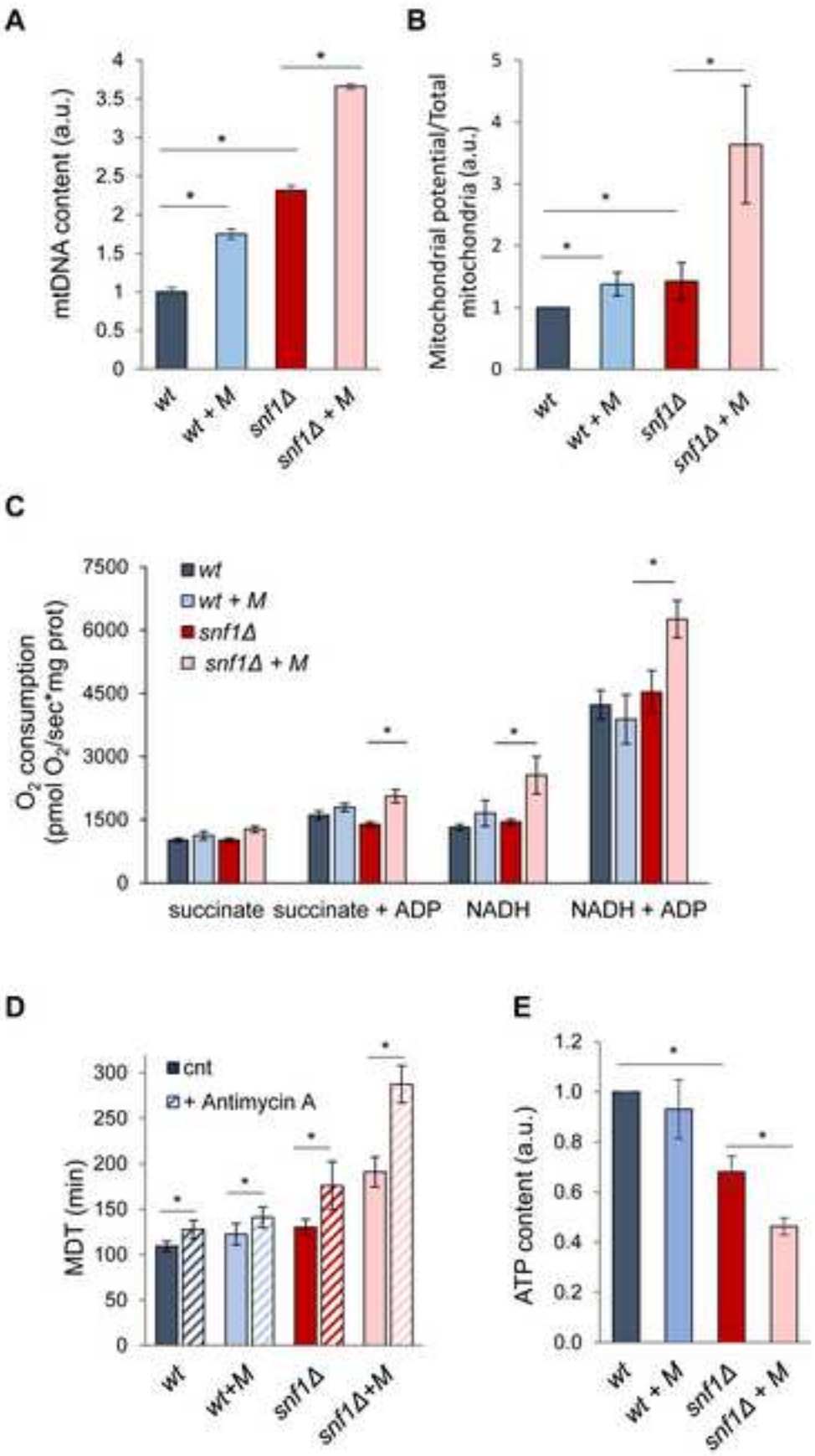

Figure5
Click here to download high resolution image

Figure 5

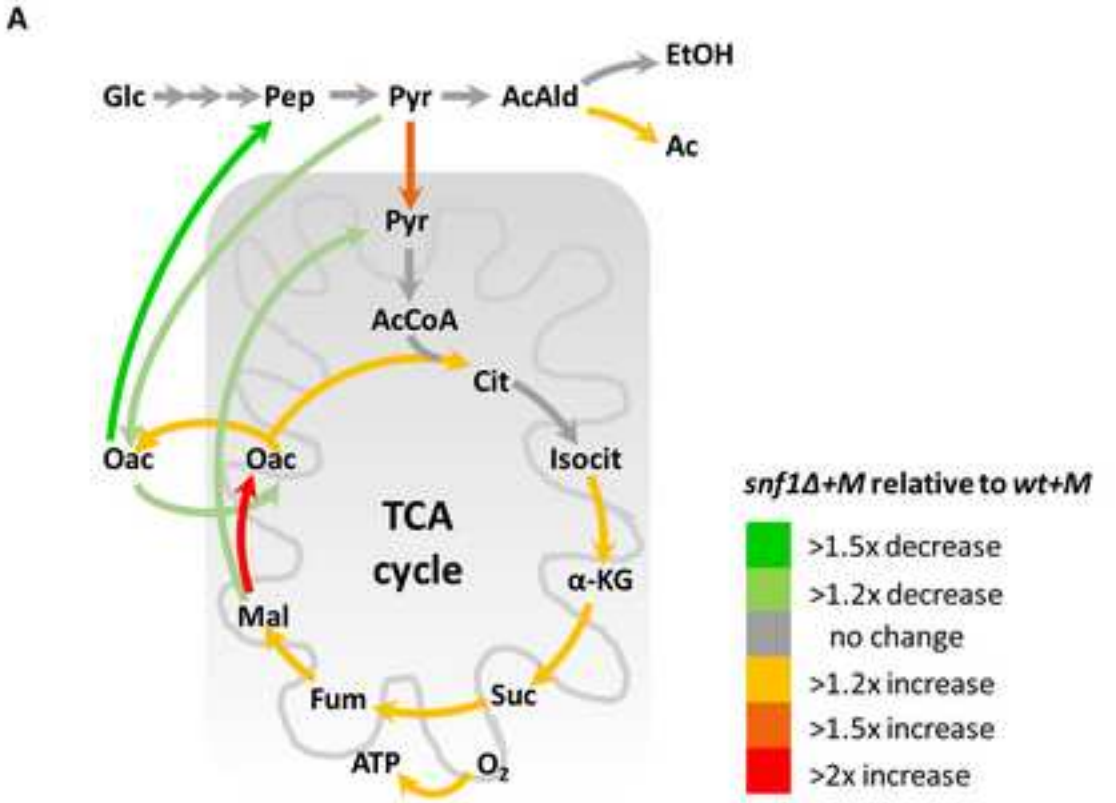

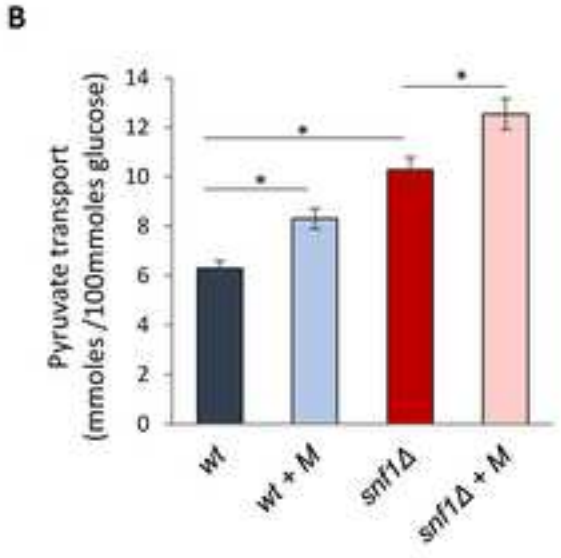

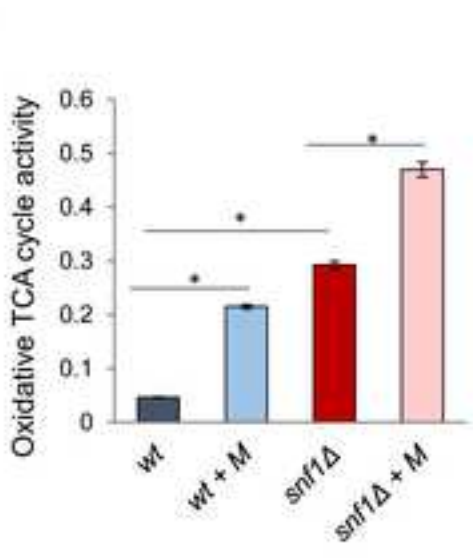

Figure6

Click here to download high resolution image

Figure 6

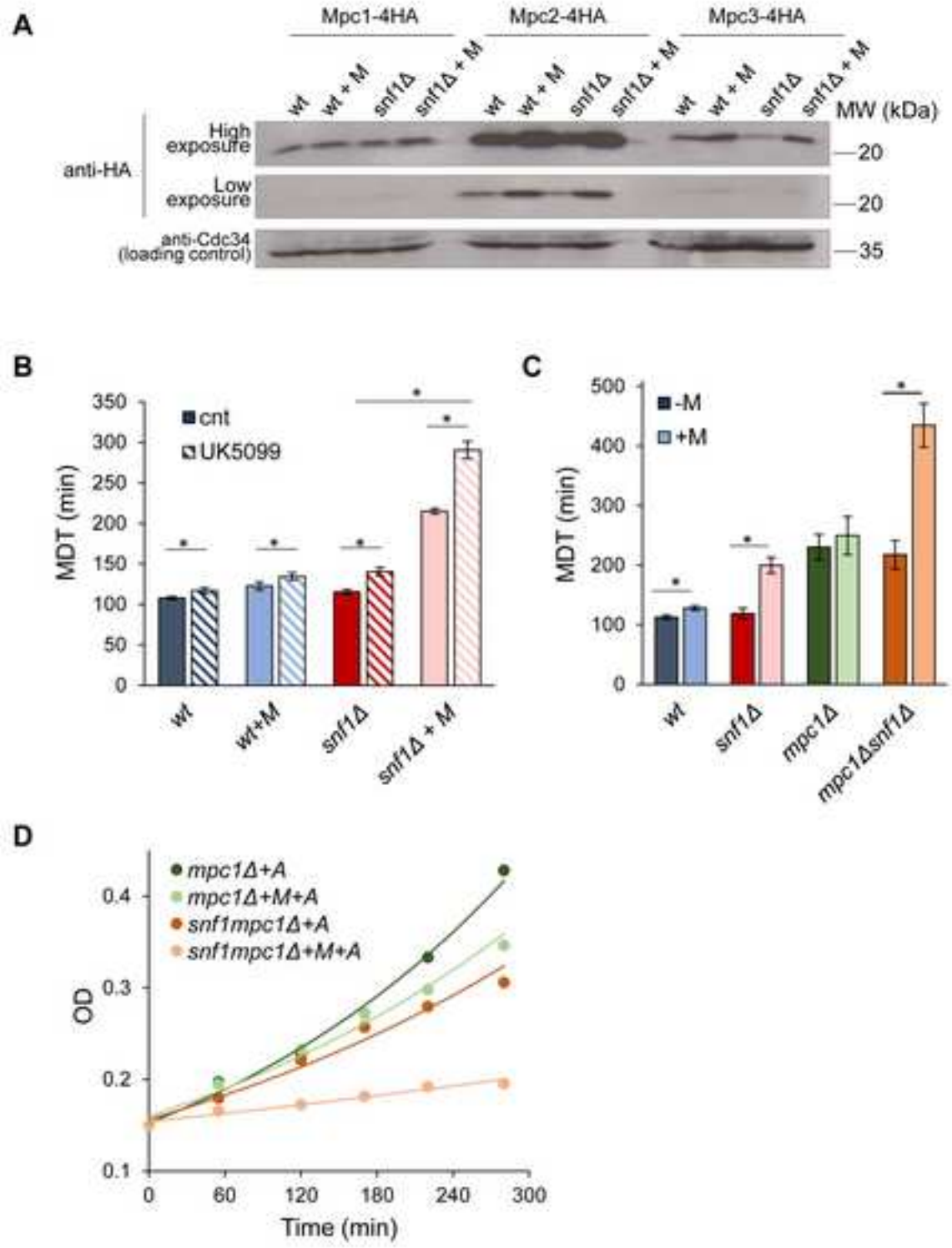

Figure7

Click here to download high resolution image

Figure 7

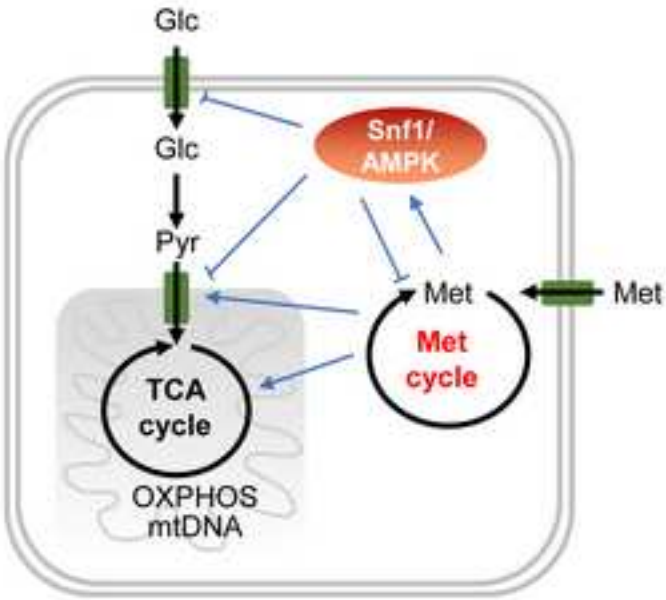

Methionine Supplementation Stimulates Mitochondrial Respiration

Supplementary Figure Legends

Figure S1. (A) Mass duplication time (MDT) of wt and *snf1Δ* cells in the presence or absence of 0.67 mM (0.1 g/l) methionine or 0.2 mM S-adenosylmethionine (SAM). * $p<0.05$. (B) Budding index of wt and *snf1Δ* cells exponentially growing in the presence or absence of 0.1 g/l methionine.

Figure S2. (A) PCA scores plot of GC/MS analysis showing the distinct clustering for the biological replicates of the four conditions, *i.e.* wt (brown squares), wt+M (brown triangles), *snf1*Δ (red squares), *snf1*Δ+M (red triangles). (B) Table of the fold changes (expressed as log2) of the heat map diagrams shown in Figure 2A.

Figure S3. Workflow of the proteomic analysis of Figure 3.

Figure S4. Lipid droplet content of wt and *snf1Δ* cells grown in the presence or absence of 0.1 g/l methionine. Data were obtained by Flow Cytometric Analysis with BODIPY staining. *$p<0.05$.

Figure S5. (A) Intracellular flux ratios (fraction of cytosolic oxaloacetate originating from cytosolic pyruvate, fraction of mitochondrial oxaloacetate derived through anaplerosis, fraction of phosphoenol-pyruvate originating from cytosolic oxaloacetate, upper and lower bounds of mitochondrial pyruvate derived through malic enzyme) (Blank and Sauer, 2004) calculated using the mass isotopomer distribution of proteinogenic amino acids and the software FIAT FLUX (Zamboni et al., 2005). (B) Relative distribution of absolute carbon fluxes in wt and *snf1Δ* grown in 2% glucose in the presence or absence of 0.1 g/L methionine. All fluxes, given in the same order in each box, are normalized to the specific glucose uptake rate, which is shown in the top inset. Relative fluxes are reported in blue for the wt, cyan for the wt+M, red for *snf1Δ* and pink for *snf1Δ*+M.

Supplementary Table Legends

Table S1. Raw data of metabolic analysis, related to Fig. 2, S2

Table S2. List of the proteins common among wt and *snf1Δ* grown in the presence or absence of 0.1 g/L methionine whose differences were statistically significant according to ANOVA test (FDR 0.05). X indicates the proteins described as mitochondrial according to Yeast Mine software and (Morgenstern et al., 2017).

Table S3. List of the proteins differentially expressed in the *snf1Δ* mutant in comparison with wt. X indicates the proteins described as mitochondrial according to Yeast Mine software and (Morgenstern et al., 2017) , Z the proteins described as mitochondrial according to (Morgenstern et al., 2017). Biological process enrichments and KEGG pathway enrichments for up-regulated and down-regulated proteins are shown.

Table S4. List of the proteins differentially expressed in wt grown in the presence or absence of 0.1 g/L methionine. X indicates the proteins described as mitochondrial according to Yeast Mine software and (Morgenstern et al., 2017), Z the proteins described as mitochondrial according to (Morgenstern et al., 2017). Biological process enrichments and KEGG pathway enrichments for up-regulated and down-regulated proteins are shown.

Table S5. List of the proteins differentially expressed in *snf1Δ* cells grown in the presence or absence of 0.1 g/L methionine. X indicates the proteins described as mitochondrial according to Yeast Mine software and (Morgenstern et al., 2017), Z the proteins described as mitochondrial according to (Morgenstern et al., 2017). Biological process enrichments and KEGG pathway enrichments for up-regulated and down-regulated proteins are shown.

Table S6. List of the proteins differentially expressed in the *snf1Δ* mutant in comparison with wt both grown in the presence of 0.1 g/L methionine. X indicates the proteins described as mitochondrial according to Yeast Mine software and (Morgenstern et al., 2017), Z the proteins

described as mitochondrial according to (Morgenstern et al., 2017). Biological process enrichments and KEGG pathway enrichments for up-regulated and down-regulated proteins are shown.

Supplementary Figure S1

A

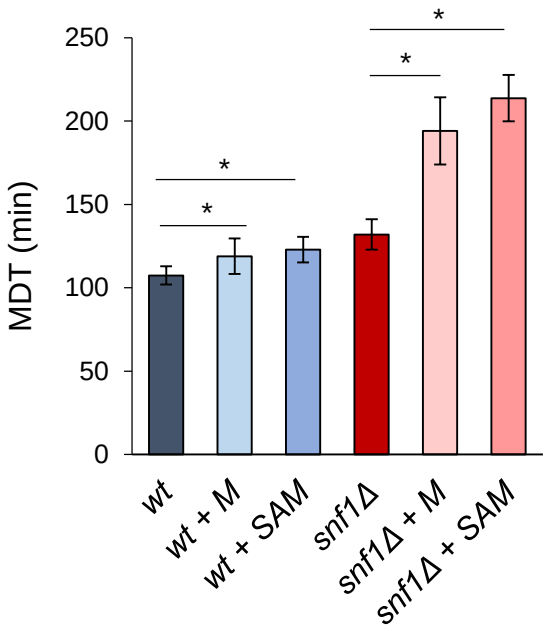

B

	Budding Index
wt	87±4%
wt+M	80±4%
snf1Δ	83±2%
snf1Δ+M	68±4%

Supplementary Figure S2

A

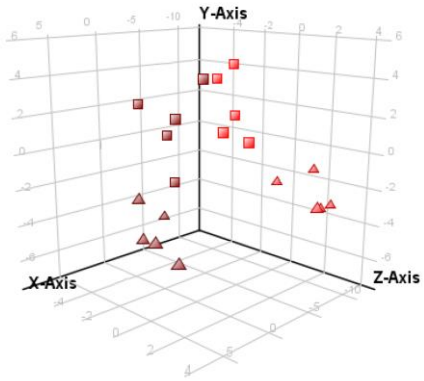

B

Glycolysis and Trehalose Cycle	wt + M / wt	snf1Δ / WT	snf1Δ + M / wt	snf1Δ + M / wt + M
Dihydroxyacetone phosphate	-0.53	-0.70	-1.39	-0.86
Fructose-1,6-diphosphate	0.03	-0.58	-0.62	-0.65
Glucose-6-phosphate	-0.72	-0.96	-1.64	-0.92
Pyruvic acid	0.11	0.58	1.14	1.03
Trehalose	0.85	2.32	7.22	6.37

Pentose phosphate pathway	wt + M / wt	snf1Δ / WT	snf1Δ + M / wt	snf1Δ + M / wt + M
6-Phosphogluconic acid	-0.49	-0.98	-0.98	-0.49
Ribose-5-phosphate	-0.33	-0.81	-1.28	-0.95

Amino acids	wt + M / wt	snf1Δ / WT	snf1Δ + M / wt	snf1Δ + M / wt + M
Alanine	0.14	0.21	0.36	0.22
Aspartic acid	-0.40	1.19	2.14	2.54
Glutamic acid	-1.34	0.77	1.21	2.55
Glutamine	-2.58	1.63	0.68	3.27
Glycine	-2.57	-0.18	-1.04	1.53
Homoserine	-0.80	0.51	0.48	1.28
Isoleucine	-2.25	0.53	-0.50	1.75
Phenylalanine	0.31	0.41	0.58	0.27
Serine	-1.08	0.65	0.36	1.44
Succinylhomoserine	-0.18	1.06	2.13	2.31
Threonine	-1.20	0.70	0.79	2.00
Valine	-3.32	0.77	-0.96	2.36
Lysine	0.46	-0.52	0.45	-0.01

Glycerol and lipids	wt + M / wt	snf1Δ / WT	snf1Δ + M / wt	snf1Δ + M / wt + M
allo-Inositol	0.39	0.33	0.16	-0.23
Capric acid	0.14	0.23	0.43	0.29
Glycerol	-0.99	0.77	0.71	1.70
Glycerol 1-phosphate	-0.20	1.05	1.75	1.95
Linoleic acid	0.15	0.25	0.47	0.32
methyl Oleate	0.80	0.58	0.42	-0.38
myo-Inositol	-0.41	0.26	0.72	1.13
Palmitic acid	0.08	0.23	0.59	0.51
Stearic acid	0.20	0.26	0.69	0.49
Stearoyl-Glycerol	1.06	0.70	1.48	0.42

TCA Cycle	wt + M / wt	snf1Δ / WT	snf1Δ + M / wt	snf1Δ + M / wt + M
Citric acid	0.18	0.80	2.10	1.92
Fumaric acid	-1.11	-0.23	0.42	1.53
Malic acid	-0.68	-0.10	0.89	1.57

Glyoxylate Cycle	wt + M / wt	snf1Δ / WT	snf1Δ + M / wt	snf1Δ + M / wt + M
Glyoxylic acid	0.02	0.14	0.34	0.32

Others	wt + M / wt	snf1Δ / WT	snf1Δ + M / wt	snf1Δ + M / wt + M
1,3-Propanediol	0.05	0.18	0.26	0.21
9H-purine-6-amine	0.45	0.36	0.30	-0.15
Acetanilide	0.06	0.18	0.27	0.21
Acetyl-glutamic acid	-1.02	0.64	1.11	2.12
Benzoic acid	-0.19	-0.75	0.08	0.26
Citraconic acid	0.49	0.71	0.89	0.40
Cysteinylglycine	0.12	0.20	0.34	0.23
Cytosine	-0.06	0.06	0.28	0.34
Dihydrouracil	-0.26	0.20	0.33	0.58
Dihydroxyphenylglycine	0.22	1.43	2.12	1.90
Malonic Acid	-1.05	0.70	0.40	1.44
Nicotinic acid	-0.13	0.76	1.40	1.53
Oxalic acid	0.11	0.28	0.40	0.29
Phenethylamine	-2.10	-0.15	-0.67	1.43
Phosphoric acid	-0.21	0.03	0.31	0.52
Pyroglutamic acid	-1.16	0.80	0.58	1.74

Urea Cycle	wt + M / wt	snf1Δ / WT	snf1Δ + M / wt	snf1Δ + M / wt + M
N-acetyl-Ornithine 2	-0.90	0.30	0.44	1.34
Ornithine	-0.81	0.90	1.09	1.90
Citrulline	-0.74	0.65	0.70	1.44

Methionine Cycle	wt + M / wt	snf1Δ / WT	snf1Δ + M / wt	snf1Δ + M / wt + M
Methionine	7.32	0.38	9.75	2.42
Homocysteine	6.17	1.11	7.55	1.38

Supplementary Figure S3

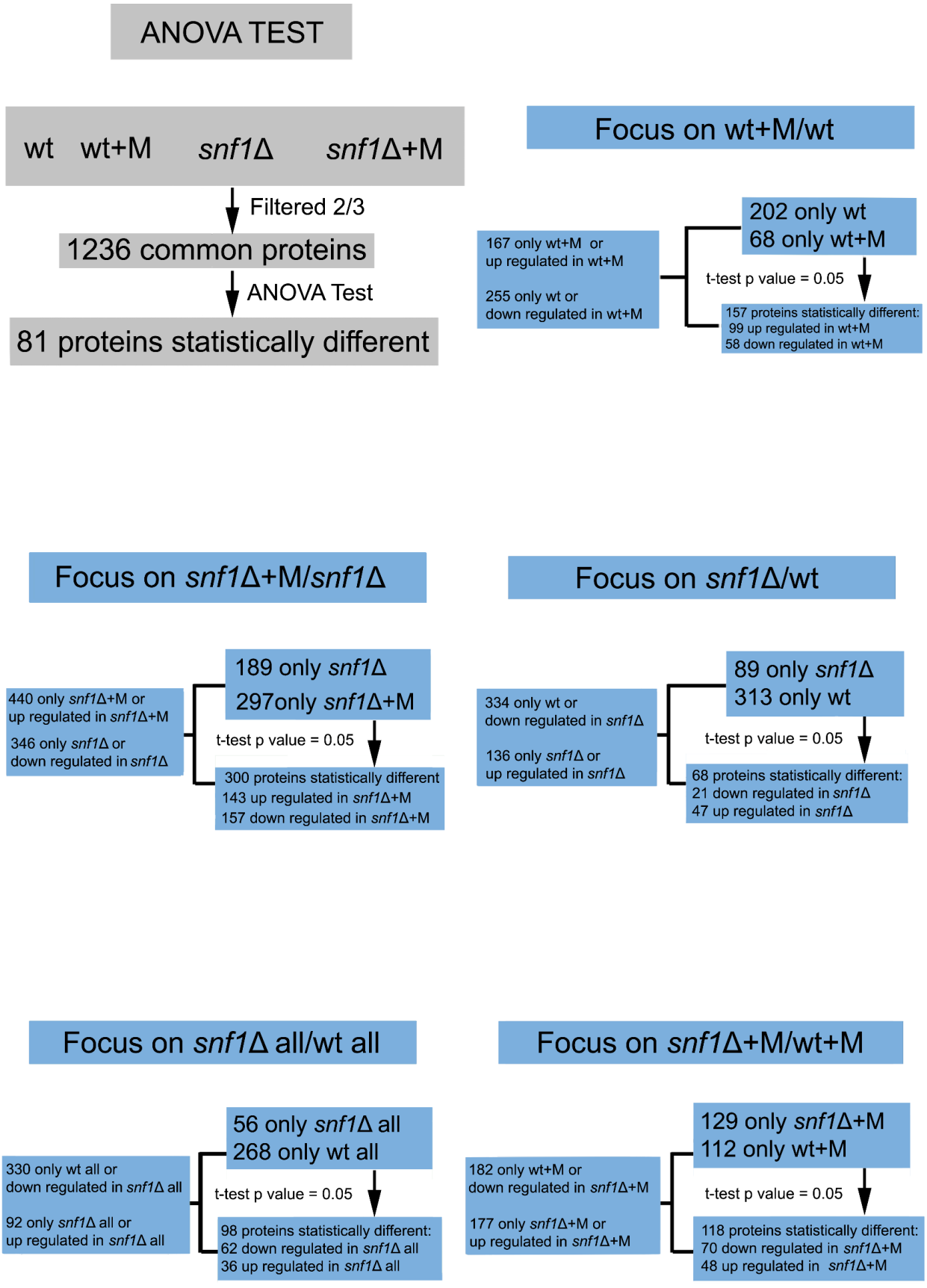

Supplementary Figure S4

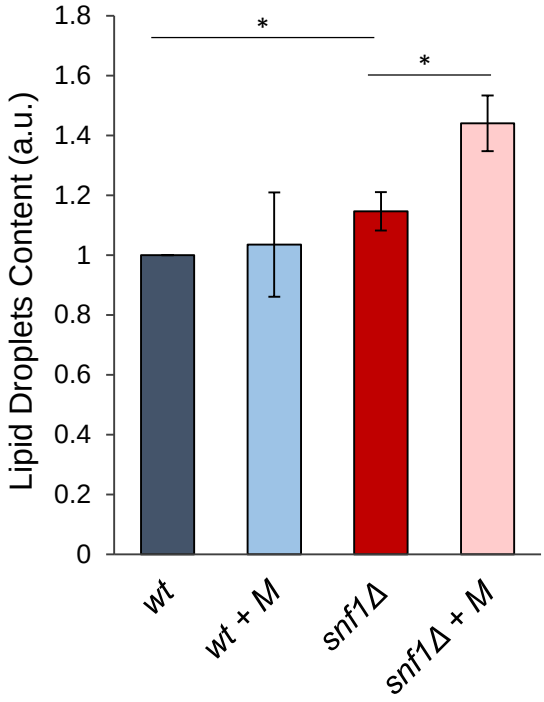

Supplementary Figure S5

A

	cytOAA from cytPYR	mtOAA from anaplerosis	malic enzyme lower bound	malic enzyme upper bound	PEP from cytOAA
	mean	*mean*	*mean*	*mean*	*mean*
wt	0.906 ± 0.028	0.954 ± 0.017	0.027 ± 0.016	0.387 ± 0.236	0.045 ± 0.013
wt + M	0.932 ± 0.027	0.785 ± 0.016	0.061 ± 0.015	0.419 ± 0.076	0.050 ± 0.040
snf1Δ	0.919 ± 0.029	0.708 ± 0.018	0.022 ± 0.016	0.070 ± 0.052	0.076 ± 0.014
snf1Δ + M	0.886 ± 0.026	0.530 ± 0.016	0.064 ± 0.016	0.235 ± 0.267	0.032 ± 0.016

B

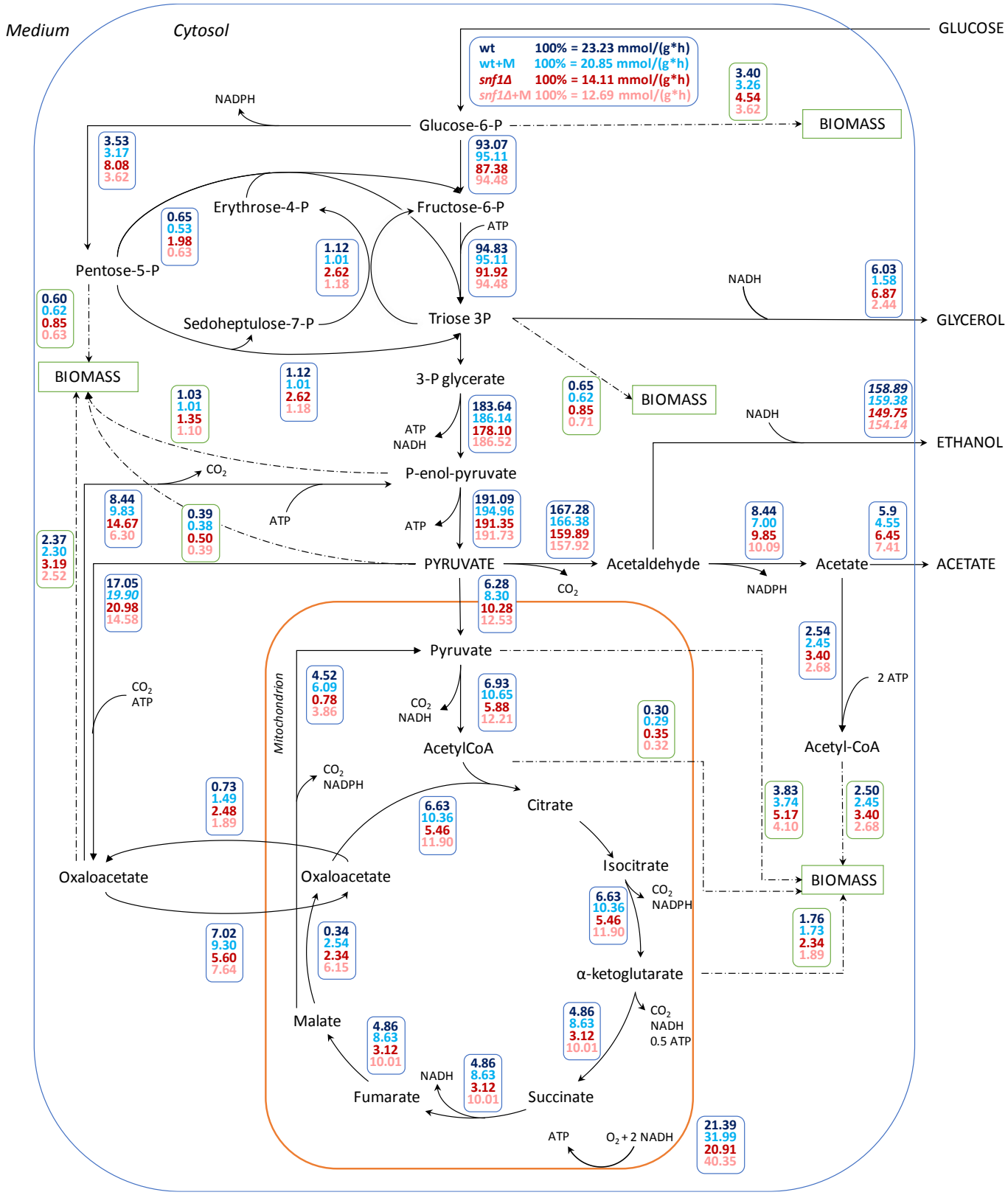

Table S1

Click here to download Supplementary Material (for online publication): Table S1_Metabolomics.xlsx

Compound	wt2A	wtB	wtC	wtD	wtE	wt+A	wt+B	wt+C
[5950] L-al	9.548866	8.930075	8.898563	8.805892	8.818842	9.059486	8.9934	9.37414
[867] malo	7.478615	6.853664	6.96526	6.991457	6.476352	6.053428	5.189891	6.99103
[5962] L-ly	13.05655	12.60086	12.70614	12.84879	12.6808	13.38929	12.53192	14.06714
[70914] N-	16.02912	14.69884	14.62217	14.876	15.08025	14.01597	13.141	15.04866
[311] citric	12.72457	11.67382	11.76415	11.90613	12.02221	12.30239	11.2854	12.95198
[791] DL-is	11.01494	9.830399	9.990864	9.955319	10.02017	7.837225	7.201081	8.766426
[328] DL-4-	5.747741	4.738308	5.238764	5.504828	5.061005	5.544423	5.529748	5.683978
[597] cytos	10.20228	8.852299	8.807695	8.807996	8.833857	8.864298	8.895675	9.26166
[985] palm	14.07733	13.40899	12.08698	13.42477	13.40085	12.0543	13.5764	13.83565
[750] glycii	12.91456	11.73319	11.74455	11.95168	12.0074	9.532492	8.960822	10.36131
[6288] L-th	11.53283	11.53806	11.7869	11.75227	11.79215	10.64357	9.625159	11.60604
[91493] 6-[	9.922213	8.856834	9.146925	9.356637	9.494328	8.548975	8.302884	9.947588
[65270] cy	9.437399	8.905895	8.912449	8.80709	8.896872	8.998928	8.944282	9.296968
[5960] asp	13.85409	13.16653	13.26074	13.24407	13.06951	13.45056	12.38728	14.10605
[439579] L	5.947633	5.030704	4.903676	5.218043	4.807577	11.28717	10.07708	12.8468
[12647] L-l	8.591826	7.590035	7.923353	7.982308	7.700054	7.197647	6.552747	8.015196
[6262] L-or	11.52903	11.20758	11.08132	11.76983	11.4785	10.66391	9.804477	11.53026
[892] myo-	8.430027	7.214488	7.71946	7.586292	7.398889	7.525226	6.715354	7.890443
[904] aceta	14.57129	13.91649	13.87782	13.8192	13.9529	13.98131	13.99648	14.26211
[5281] stea	15.89922	15.22218	13.74679	15.32808	15.2602	14.03113	15.52341	15.79301
[33032] L-g	13.94971	12.69174	12.78355	12.83867	13.09004	11.99398	10.61809	13.3365
[7427] D-(+	7.757687	6.972048	7.230052	7.183782	7.341092	8.161732	7.580984	8.868601
[24699] 1-s	10.01086	9.184942	8.497473	11.45408	9.456961	8.627205	11.73563	11.99827
[6137] L-m	11.93181	10.68636	10.80899	10.90564	10.94911	12.95597	11.97455	13.65359
[5951] L-se	13.47065	12.74963	12.85502	12.90185	12.48064	12.03461	10.55458	12.93794
[5280450]	12.99612	12.41145	12.37187	12.44687	12.49737	12.52268	12.56889	12.8732
[243] benz	13.2907	12.20857	12.48434	12.6332	12.7822	12.4202	12.13962	12.8354
[439167] D	9.778563	8.86767	9.162344	9.358911	9.429152	8.548975	8.346555	9.872774
[2969] cap	10.52322	9.781584	9.807175	10.01041	10.02015	9.908701	10.13129	10.50875
[971] oxali	6.705238	6.161531	5.943542	6.101486	6.260603	6.066575	6.247668	6.523795
[994] Phen	5.453515	4.65935	5.352079	5.083129	4.748458	5.638798	5.350328	5.494621
[938] nicot	9.460487	8.343735	8.599093	8.673839	8.581425	8.594143	7.967837	9.295187
[738] L-glu	12.05924	10.88788	11.4881	11.37614	10.58505	9.008822	7.814986	9.593386
[5960] asp	12.78528	10.74884	10.89669	11.12463	11.49143	11.24862	9.962876	12.35226
[1060] pyr	8.901827	8.005096	8.157452	8.134126	8.506537	8.428444	7.846849	9.143993
[10267] fru	6.090731	6.252999	4.968256	6.658807	7.742334	5.347035	5.206958	7.378145
[92824] D-	8.907558	7.538001	7.679023	7.709544	7.819492	7.37578	6.481913	8.103207
[439232] N	11.1338	9.486794	9.365047	9.754441	10.37804	9.029093	8.224179	10.14431
[638129] c	8.362603	8.124504	7.700724	8.284537	8.407906	8.210753	8.623206	8.986523
[10442] 1,3	10.77517	10.1392	10.1116	10.07462	10.15803	10.20518	10.20393	10.47639
[439958] D	11.64856	10.78916	10.96511	11.54069	11.93806	10.50642	9.845544	11.8057
[754] glyce	9.105211	7.83145	7.780546	7.914153	8.223545	7.920092	7.720878	8.531666
[892] allo-i	7.493501	6.771367	9.00119	7.662946	6.859564	9.050776	7.769261	8.03162
[443586] 3	6.687738	6.221756	5.7753	6.445354	6.761925	6.181258	6.037915	7.368023
[760] glyox	10.23754	9.647776	9.363968	9.56005	9.701389	9.407194	9.605592	9.910625
[649] 5,6-d	15.04297	14.0637	14.21313	14.17358	14.2047	14.18281	13.80712	14.4406
[33032] L-g	13.64562	13.08451	12.8704	13.17358	13.21179	11.97056	10.53225	13.11682
[668] dihyc	8.208009	7.105441	7.323817	7.547369	7.760975	6.952872	6.342217	7.791546
[1004] pho	14.35853	13.42785	13.59234	13.64763	13.92335	13.50151	13.21352	13.93939

Table S2

Click here to download Supplementary Material (for online publication): Table S2_Anova.xls

Protein ID	*Gene*	*Protein names*	*Length*
P38631	FKS1_YEAST	1,3-beta-glucan synthase component FKS1 (EC 2.4	1876
P32621	GDA1_YEAST	Guanosine-diphosphatase (GDPase) (EC 3.6.1.42)	518
P53171	GEP7_YEAST	Genetic interactor of prohibitin 7, mitochondrial	287
P41921	GSHR_YEAST	Glutathione reductase (GR) (GRase) (EC 1.8.1.7)	483
P21954	IDHP_YEAST	Isocitrate dehydrogenase [NADP], mitochondrial (	428
P32466	HXT3_YEAST	Low-affinity glucose transporter HXT3	567
P28241	IDH2_YEAST	Isocitrate dehydrogenase [NAD] subunit 2, mitoch	369
P30605	ITR1_YEAST	Myo-inositol transporter 1	584
P06208	LEU1_YEAST	2-isopropylmalate synthase (EC 2.3.3.13) (Alpha-I	619
P42838	LEM3_YEAST	Alkylphosphocholine resistance protein LEM3 (Br	414
P40513	MAM33_YEAST	Mitochondrial acidic protein MAM33	266
P17505	MDHM_YEAST	Malate dehydrogenase, mitochondrial (EC 1.1.1.3	334
Q12285	MDY2_YEAST	Ubiquitin-like protein MDY2 (Golgi to ER traffic pr	212
P40185	MMF1_YEAST	Protein MMF1, mitochondrial (Isoleucine biosynth	145
P33201	MRT4_YEAST	Ribosome assembly factor MRT4 (mRNA turnover	236
P10507	MPPB_YEAST	Mitochondrial-processing peptidase subunit beta	462
Q07938	MTAP_YEAST	S-methyl-5'-thioadenosine phosphorylase (EC 2.4	337
P49954	NIT3_YEAST	Probable hydrolase NIT3 (EC 3.5.-.-)	291
P32340	NDI1_YEAST	Rotenone-insensitive NADH-ubiquinone oxidored	513
P32860	NFU1_YEAST	NifU-like protein, mitochondrial	256
Q12428	PRPD_YEAST	Probable 2-methylcitrate dehydratase (2-MC deh	516
P07257	QCR2_YEAST	Cytochrome b-c1 complex subunit 2, mitochondri	368
P37299	QCR10_YEAST	Cytochrome b-c1 complex subunit 10 (Complex III	77
P00128	QCR7_YEAST	Cytochrome b-c1 complex subunit 7 (Complex III s	127
P07256	QCR1_YEAST	Cytochrome b-c1 complex subunit 1, mitochondri	457
P0CX41	RL23A_YEAST	60S ribosomal protein L23-A (L17a) (Large ribosor	137
P36528	RM17_YEAST	54S ribosomal protein L17, mitochondrial (Mitoch	281
P20435	RPAB2_YEAST	DNA-directed RNA polymerases I, II, and III subun	155
Q12487	RM23_YEAST	54S ribosomal protein L23, mitochondrial (Mitoch	163
Q00711	SDHA_YEAST	Succinate dehydrogenase [ubiquinone] flavoprote	640
P21825	SEC62_YEAST	Translocation protein SEC62 (Sec62/63 complex 3	274
Q99287	SEY1_YEAST	Protein SEY1 (EC 3.6.5.-) (Synthetic enhancer of Y(	776
P00445	SODC_YEAST	Superoxide dismutase [Cu-Zn] (EC 1.15.1.1)	154
P00447	SODM_YEAST	Superoxide dismutase [Mn], mitochondrial (EC 1.1	233
P0CF17	U5072_YEAST	UPF0507 protein YML002W	737
P08067	UCRI_YEAST	Cytochrome b-c1 complex subunit Rieske, mitoch	215
P32316	ACH1_YEAST	Acetyl-CoA hydrolase (EC 3.1.2.1) (Acetyl-CoA dea	526
P32317	AFG1_YEAST	Protein AFG1	509
P23180	AIM17_YEAST	Probable oxidoreductase AIM17 (EC 1.14.11.-) (Al	465
Q01976	ADPP_YEAST	ADP-ribose pyrophosphatase (EC 3.6.1.13) (ADP-r	231
Q04728	ARGJ_YEAST	Arginine biosynthesis bifunctional protein ArgJ, m	441
P07251	ATPA_YEAST	ATP synthase subunit alpha, mitochondrial	545
Q12165	ATPD_YEAST	ATP synthase subunit delta, mitochondrial (F-ATP	160
P05626	ATPF_YEAST	ATP synthase subunit 4, mitochondrial	244
P00830	ATPB_YEAST	ATP synthase subunit beta, mitochondrial (EC 3.6.	511
P32451	BIOB_YEAST	Biotin synthase, mitochondrial (EC 2.8.1.6)	375
P14066	CBS1_YEAST	Cytochrome b translational activator protein CBS1	229

Table S3

Click here to download Supplementary Material (for online publication): Table S3_snf1-wt.xlsx

Protein ID	*Gene*
N1NWR5	SIL1
N1P175	AIM25
N1P9Y0	PDX1
N1P4D6	ZIM17
N1P520	QCR6
N1P1I4	SEC72
N1P2V2	ZRT1
N1P9X9	CRH1
N1P227	AIM23
N1P1U0	CCW14
N1P7X1	ATP16
N1PAC3	PST1
N1NVJ9	RPL43A
N1NZ71	YBT1
N1P1X3	GEP7
N1P797	ECM11
N1P7M3	ADE1
N1P998	TMA108
N1NYB6	APS1
P32366	VMA6
N1P2G2	SDP1
Q99380	OST4
P34166	MFA2
P54114	ALD3
Q3E752	YPR036W-A
P40089	LSM5
Q3E795	YLR361C-A
Q12306	SMT3
Q06139	YLR346C
P22943	HSP12
P38841	YHR138C
P10663	MRP2
P27999	RPB9
P26755	RFA3
P38155	PAU24
P40045	TDA2
P38783	FYV4
Q12127	CCW12

Table S4

Click here to download Supplementary Material (for online publication): Table S4_wt+M-wt.xlsx

Protein ID	*Gene*	*Protein names*
		Up-regulated in wt+M
P53171	GEP7	Genetic interactor of prohibitin 7, mitochondrial
P14742	GFA1	Glutamine--fructose-6-phosphate aminotransferase [isomerizing] (
P48015	GCV1	Aminomethyltransferase, mitochondrial (Glycine cleavage system
P38988	GGC1	Mitochondrial GTP/GDP carrier protein 1
P21954	IDP1	Isocitrate dehydrogenase [NADP], mitochondrial (IDH) (IDP) (NADP
P19882	HSP60	Heat shock protein 60, mitochondrial (CPN60) (P66) (Stimulator fac
P28241	IDH2	Isocitrate dehydrogenase [NAD] subunit 2, mitochondrial (Isocitric
P28834	IDH1	Isocitrate dehydrogenase [NAD] subunit 1, mitochondrial (Isocitric
P39522	ILV3	Dihydroxy-acid dehydratase, mitochondrial (DAD) (2,3-dihydroxy a
P06208	LEU4	2-isopropylmalate synthase (Alpha-IPM synthase) (Alpha-isopropyl
P40513	MAM33	Mitochondrial acidic protein MAM33
P17505	MDH1	Malate dehydrogenase, mitochondrial
P40185	MMF1	Protein MMF1, mitochondrial (Isoleucine biosynthesis and mainten
P38162	MIX23	Mitochondrial intermembrane space cysteine motif-containing prot
Q08818	MSC6	Meiotic sister-chromatid recombination protein 6, mitochondrial
P23641	MIR1	Mitochondrial phosphate carrier protein (Mitochondrial import rec
Q12117	MRH1	Protein MRH1 (Membrane protein related to HSP30)
P11914	MAS2	Mitochondrial-processing peptidase subunit alpha (Alpha-MPP)
P10507	MAS1	Mitochondrial-processing peptidase subunit beta (Beta-MPP) (PEP
P25270	MRM1	rRNA methyltransferase 1, mitochondrial (21S rRNA (guanosine(22
P53166	MRH4	ATP-dependent RNA helicase MRH4, mitochondrial (Mitochondrial
P32340	NDI1	Rotenone-insensitive NADH-ubiquinone oxidoreductase, mitochon
P32860	NFU1	NifU-like protein, mitochondrial
P38848	PEX28	Peroxisomal membrane protein PEX28 (Peroxin-28)
Q12428	PDH1	Probable 2-methylcitrate dehydratase (2-MC dehydratase) ((2S,3S)
P07257	QCR2	Cytochrome b-c1 complex subunit 2, mitochondrial (Complex III sub
P37299	QCR10	Cytochrome b-c1 complex subunit 10 (Complex III subunit 10) (Com
P00128	QCR7	Cytochrome b-c1 complex subunit 7 (Complex III subunit 7) (Compl
P07256	COR1	Cytochrome b-c1 complex subunit 1, mitochondrial (Complex III sub
P36528	MRPL17	54S ribosomal protein L17, mitochondrial (Mitochondrial large ribo
P32388	MRP49	54S ribosomal protein MRP49, mitochondrial (Mitochondrial large
Q06678	MRPL35	54S ribosomal protein L35, mitochondrial (Mitochondrial large ribo
Q00711	SDH1	Succinate dehydrogenase [ubiquinone] flavoprotein subunit, mitoch
P38827	SET1	Histone-lysine N-methyltransferase, H3 lysine-4 specific (COMPASS
Q02208	TOF2	Topoisomerase 1-associated factor 2
P08067	RIP1	Cytochrome b-c1 complex subunit Rieske, mitochondrial (Complex
P07246	ADH3	Alcohol dehydrogenase 3, mitochondrial (Alcohol dehydrogenase I

Table S5

Click here to download Supplementary Material (for online publication): Table S5_snf1+M-snf1.xlsx

Protein ID	*Gene*
P36141	FMP46
P33893	PET112
P00360	TDH1
P53171	GEP7
P39726	GCV3
P41921	GLR1
P38715	GRE3
P32191	GUT2
P21954	IDP1
P28241	IDH2
P33416	HSP78
Q6Q560	ISD11
P36775	PIM1
P06208	LEU4
P40513	MAM33
P17505	MDH1
Q12230	LSP1
P36112	MIC60
P32787	MGM101
Q99257	MEX67
P25573	MGR1
P38341	MIC12
P50945	MIC27
Q03104	MSC1
P40185	MMF1
P40364	MPM1
Q08818	MSC6
P10507	MAS1
Q07938	MEU1
P40215	NDE1
P32340	NDI1
P32860	NFU1
P38921	PET8
P40530	PKP1
P35999	OCT1
P41903	TES1
Q12428	PDH1
P07257	QCR2
P37299	QCR10
P00128	QCR7
P07256	COR1

Table S6

Click here to download Supplementary Material (for online publication): Table S6_snf1+M-wt+M.xlsx

Protein ID	*Gene*	*Protein names*
		Down-regulated in snf1 Δ+M
P38631	FKS1	1,3-beta-glucan synthase component FKS1 (1,3-beta-D-glucan-UD
P32621	GDA1	Guanosine-diphosphatase (GDPase)
P16474	KAR2	78 kDa glucose-regulated protein homolog (GRP-78) (Immunoglo
P47042	IKS1	Probable serine/threonine-protein kinase IKS1 (IRA1 kinase supp
P27810	KTR1	Alpha-1,2 mannosyltransferase KTR1
P42838	LEM3	Alkylphosphocholine resistance protein LEM3 (Brefeldin-A sensiti
Q12404	MPD1	Protein disulfide-isomerase MPD1
P33201	MRT4	Ribosome assembly factor MRT4 (mRNA turnover protein 4)
P42934	PMT6	Dolichyl-phosphate-mannose--protein mannosyltransferase 6
P33333	SLC1	Probable 1-acyl-sn-glycerol-3-phosphate acyltransferase (1-AGP a
P31382	PMT2	Dolichyl-phosphate-mannose--protein mannosyltransferase 2
P53131	PRP43	Pre-mRNA-splicing factor ATP-dependent RNA helicase PRP43 (He
P25560	RER1	Protein RER1 (Retention of ER proteins 1)
P10964	RPA190	DNA-directed RNA polymerase I subunit RPA190 (EC 2.7.7.6) (DN
P21825	SEC62	Translocation protein SEC62 (Sec62/63 complex 30 kDa subunit)
Q08199	SIL1	Nucleotide exchange factor SIL1 (Protein SLS1)
Q99287	SEY1	Protein SEY1 ((Synthetic enhancer of YOP1 protein)
P53165	SGF73	SAGA-associated factor 73 (73 kDa SAGA-associated factor) (SAG
P35209	SPT21	Protein with a role in transcriptional silencing; required for norma
Q12133	SPC3	Signal peptidase complex subunit SPC3 (Microsomal signal peptid
Q12513	TMA17	Translation machinery-associated protein 17 (ATPase-dedicated c
P36017	VPS21	Vacuolar protein sorting-associated protein 21 (GTP-binding prot
P21576	VPS1	Vacuolar protein sorting-associated protein 1
P21147	OLE1	Acyl-CoA desaturase 1 (Delta 9 fatty acid desaturase) (Fatty acid
P53730	ALG12	Dol-P-Man:Man(7)GlcNAc(2)-PP-Dol alpha-1,6-mannosyltransfera
P15703	BGL2	Glucan 1,3-beta-glucosidase (Exo-1,3-beta-glucanase) (GP29) (Sol
P41810	SEC26	Coatomer subunit beta (Beta-coat protein) (Beta-COP)
O13547	CCW14	Covalently-linked cell wall protein 14 (Inner cell wall protein)
P24871	CLB4	G2/mitotic-specific cyclin-4
P32891	DLD1	D-lactate dehydrogenase [cytochrome] 1, mitochondrial (D-lactat
P25340	ERG4	Delta(24(24(1)))-sterol reductase (C-24(28) sterol reductase) (Ste
P32462	ERG24	Delta(14)-sterol reductase (C-14 sterol reductase) (Sterol C14-red
P53337	ERV29	ER-derived vesicles protein ERV29
P43555	EMP47	Protein EMP47 (47 kDa endomembrane protein) (Endosomal P44
P32476	ERG1	Squalene monooxygenase (Squalene epoxidase) (SE)
Q12452	ERG27	3-keto-steroid reductase
Q05040	FAR8	Factor arrest protein 8
P43613	ERJ5	ER-localized J domain-containing protein 5
P32339	HMX1	Heme-binding protein HMX1
P27476	NSR1	Nuclear localization sequence-binding protein (p67)
P38837	NSG1	Protein involved in regulation of sterol biosynthesis
P46964	OST2	Dolichyl-diphosphooligosaccharide--protein glycosyltransferase s
Q99380	OST4	Dolichyl-diphosphooligosaccharide--protein glycosyltransferase s
P53224	ORM1	Protein that mediates sphingolipid homeostasis
P25343	RVS161	Reduced viability upon starvation protein 161
Q03529	SCS7	Ceramide very long chain fatty acid hydroxylase SCS7 (Ceramide

***Conflict of Interest**

Click here to download Conflict of Interest: coi_disclosure.pdf